ORNL/SPR-2024/3544

Recent High-Burnup LOCA Testing at Oak Ridge National Laboratory

Nathan Capps
Yong Yan
Jason Harp
Mackenzie Ridley
Robert Salko Jr.

September 2024

OAK RIDGE National Laboratory

ORNL IS MANAGED BY UT-BATTELLE LLC FOR THE US DEPARTMENT OF ENERGY

ORNL/SPR-2024/3544

Advanced Fuels Campaign

RECENT HIGH-BURNUP LOCA TESTING AT OAK RIDGE NATIONAL LABORATORY

Nathan Capps
Yong Yan
Jason Harp
Mackenzie Ridley
Robert Salko Jr.

September 2024

Prepared by
OAK RIDGE NATIONAL LABORATORY
Oak Ridge, TN 37831
managed by
UT-BATTELLE LLC
for the
US DEPARTMENT OF ENERGY
under contract DE-AC05-00OR22725

CONTENTS

LIST OF FIGURES

LIST OF TABLES

ABSTRACT

To improve fuel cycle economics, increasing the fuel burnup limit in light-water reactors requires a solid technical foundation. Observations from experiments at Halden and Studsvik highlighted severe fuel fragmentation during loss-of-coolant-accident (LOCA) conditions, indicating a need for further technical considerations. These experiments suggest that the fragmentation threshold for high-burnup fuel might be influenced by pre-transient power levels. Consequently, additional LOCA test data are essential to complement existing findings and to deepen our understanding. Oak Ridge National Laboratory's Severe Accident Test Station has been instrumental in advancing knowledge about high-burnup fuel fragmentation, relocation, and dispersal. This milestone report details two high-burnup LOCA tests designed to evaluate the effects of terminal temperature and grid spacers (or cladding restraints) on fuel fragmentation and relocation susceptibility. In addition, BISON fuel performance modeling and out-of-cell benchmark testing were conducted to better interpret the in-cell test results. These tests were developed in collaboration with fuel vendors to ensure that the results provide valuable data for topical reports and support the Nuclear Regulatory Commission's review.

1. INTRODUCTION

Nuclear power currently accounts for approximately 20% of total electricity generation in the United States and over 10% globally. There is a growing reliance on nuclear energy to achieve our nation's ambitious goal of reaching net-zero carbon emissions by 2050. These objectives have significantly increased pressure on existing nuclear industry to extend plants' operational licenses and enhance their operational efficiencies. These goals are crucial because they serve as a vital bridge until new light-water and advanced reactors can be developed and deployed, all while bolstering the supply of carbon-free energy to meet domestic demands. Given this urgency and importance, the US Department of Energy must formulate a comprehensive strategy to support, preserve, and extend the operational licenses of our existing nuclear fleet.

Presently, operational costs primarily stem from plant operation and maintenance (O&M), coupled with fuel costs that are influenced by materials and reactor core designs. These factors, compounded by heavily subsidized renewable energy markets, create a challenging economic environment. In response, the nuclear industry crafted a strategic blueprint aimed at fortifying nuclear power's economic sustainability by building on past initiatives within the nuclear sector. For instance, efforts in the mid-2000s aimed to eliminate fuel failures by 2010, thereby reducing costs associated with reactor shutdowns and fuel replacement. Subsequent goals included reducing operating costs by 30% before 2020 to increase nuclear energy's competitiveness.

Core design parameters, such as the enrichment limit of 5% ^{235}U and a peak rod average burnup limit of 62 GWd/tU, place constraints on cycle lengths. Extending cycle lengths reduces outages and maintenance costs, making higher burnup and enrichment economically beneficial. To extend PWR fuel cycles to 24 months, the peak rod average burnup must reach 75 GWd/MTU, with a peak pellet burnup approximately 12% higher than the rod average. Utilities are expected to achieve these burnup extensions while adhering to current safety criteria and leveraging existing licensing practices. While this process is generally straightforward, it involves ensuring that core geometry supports adequate cooling and revising accident source term analyses. The issues of core geometry and cooling are addressed separately, as discussed in the next paragraph, and are distinct from concerns about flow blockage due to cladding ballooning, which was thoroughly studied and deemed inconsequential in the 1980s. However, the revision of accident source term analyses will likely need to consider fuel fragmentation, relocation, and dispersion (FFRD).

To date, Oak Ridge National Laboratory (ORNL) has been at the forefront of domestic efforts to extend burnup beyond 62 GWd/tU and maintains strong collaborations with the international Studsvik Cladding

Integrity Project (SCIP), which has been conducting testing on high-burnup materials for over a decade. ORNL utilizes the Severe Accident Test Station (SATS) to test high-burnup commercially irradiated materials. Recently, ORNL performed two tests specifically aimed at addressing critical data gaps in the current high-burnup loss-of-coolant accident (LOCA) data set. Historically, LOCA testing has replicated the high-temperature oxidation tests conducted by Argonne National Laboratory (Argonne). These tests involved heating cladding segments from 300°C to 1000–1200°C at a rate of 5°C/s, simulating the "hot rod" conditions during a large break LOCA. However, high-burnup fuel operates at lower powers and is unlikely to reach temperatures comparable to those in hot rod tests. Testing high-burnup fuel rods under these traditional conditions could yield overly conservative results. Consequently, the first LOCA test documented in this report focuses on terminal temperatures that are more representative of high-burnup LOCA conditions.

The second LOCA test described in this report examined how cladding structural features influence cladding deformation and how this deformation affects fuel fragmentation and relocation. Recent analytical results suggest that cladding deformation during a LOCA is locally reduced near grid spacers or mixing veins. This behavior is attributed to the reduced local power due to these structural features and the enhanced mixing they promote. As a result, temperatures in these regions are lower, which limits cladding deformation. The analysis also indicates that these assembly structural features may impose additional mechanical constraints, further reducing deformation and potentially limiting fuel fragmentation and relocation. The purpose of this experiment was to validate these analytical findings and provide essential data to support high burnup safety assessments.

2. H.B. ROBINSON

2.1 TEST RESULTS

A LOCA test was conducted to evaluate the effects of terminal temperature on a sample taken from a fuel rod irradiated in the H.B. Robinson light-water reactor. This test, designated HBR#2, is a follow-up to the previous LOCA test on similar fuel, known as HBR#1. Detailed information about the fuel rod and test conditions can be found in

Table 1, and the detailed fuel operating and performance conditions have been previously reported in McKinney et al. [1].

There are two key differences between the HBR#1 and HBR#2 tests. First, HBR#1 reached a terminal temperature of 1000°C, whereas HBR#2 achieved a terminal temperature of 900°C. Second, the rodlet lengths differed: HBR#1 was 12 in. long, while HBR#2 was approximately 7.9 in. long. The shorter length of HBR#2 more accurately represents the span between grids in the upper regions of the core, where rupture is most likely to occur. Additionally, the SATS system provides a 4 in. uniform axial temperature distribution in the center of the furnace, ensuring that the sample in HBR#2 experienced consistent conditions within the heated region.

Table 1. Summary of the HBR#2 LOCA test conditions in comparison to HBR#1 [2]

Parameter	HBR#1	HBR#2
Fuel	H.B. Robinson	H.B. Robinson
Materials	Zry-4	Zry-4
Father rod burnup (GWd/MTU)	66.5	66.5
Rodlet burnup (GWd/MTU)	~71	~71
Rodlet Length (cm)	~30	~20
Outside diameter (mm)	10.77	10.77
Wall thickness (mm)	0.76	0.76
Environment	Flowing Steam	Flowing Steam
Internal pressure at 300°C (MPa)	8.27	8.27
Temperature ramp from 300°C (°C/s)	5	5
Hold temperature (°C)	1,000	900
Hold time (s)	120	120
Cool-down rate to 800°C (°C/s)	3	3

The HBR#2 online thermocouple and pressure measurements are shown in Figure 1. The sample was pressurized to 8.27 MPa (1,200 psi) at 100°C to assess its pressure-holding capability. Although a minor leak was detected, it was deemed negligible and unlikely to affect the LOCA test results. The sample was then heated to 300°C and maintained at this temperature for 10 min. Additional gas was introduced into the system shortly after 400 s to restore the pressure to 8.27 MPa (1,200 psi). The LOCA transient commenced around 700 s, as indicated by a temperature increase recorded by the thermocouples. The sample was heated at a rate of 5°C/s to 900°C and held at this temperature for 120 s before the furnace was turned off. For most of the transient, the pressure remained stable. However, between approximately 825 and 850 s, the pressure began to decrease gradually. This drop in pressure was attributed to cladding failure, as confirmed by a sudden deviation in the thermocouple readings, which were 870°C and 850°C at the time of failure. This slower pressure decline contrasts with previous observations, where the pressure typically decreased more rapidly from the test pressure to near-atmospheric levels within about 60 s. The observed slower pressure drop in HBR#2 suggests there may have been inadequate gas communication between the rodlet and the external gas lines. At 925 s, the pressure suddenly dropped when the sample fell from the fixture where it was held during the test and landed at the bottom of the quartz tube. The thermocouples remained in place and continued to record the furnace temperature until the hold was complete and the furnace began to cool at 988 s.

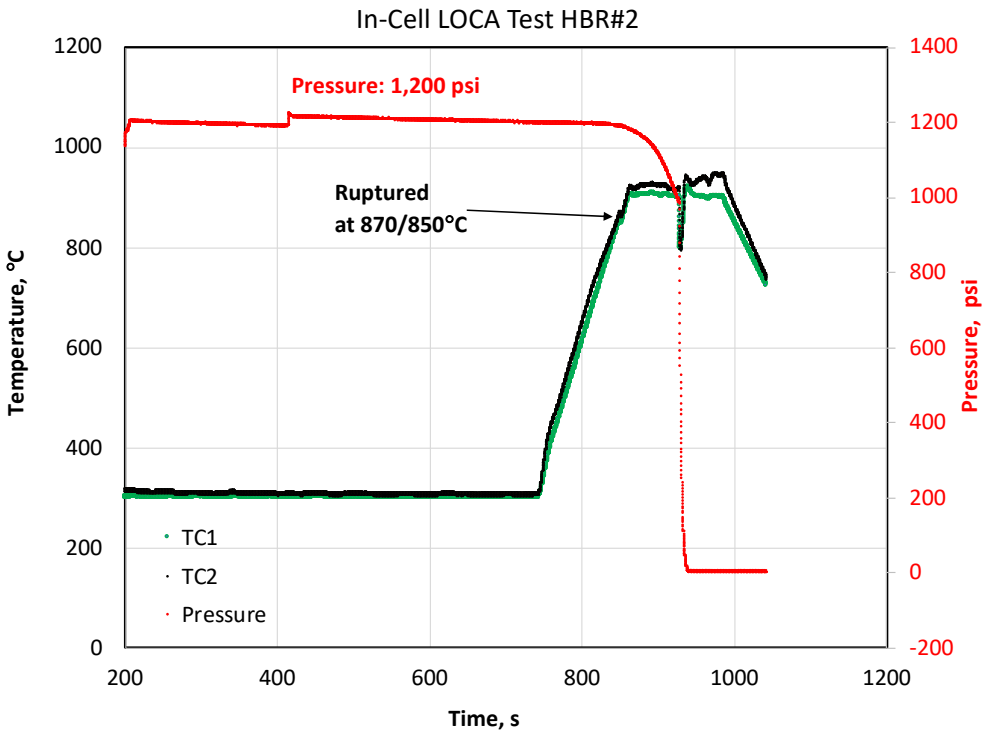

Figure 1. HBR#2 time-dependent temperature and pressure measurements during in-cell test.

The results from the HBR#2 test are presented in Table 2 and compared with the results from the HBR#1 test. A key observation is the difference in rupture temperature: HBR#1 ruptured at 770°C, whereas HBR#2 ruptured in the range of 850–870°C. This discrepancy is unexpected given that both tests used material from the same rod and maintained consistent internal pressures. Another notable difference is in balloon strain. HBR#1 exhibited a peak strain of 25%, whereas HBR#2 showed a peak strain of 10%. The axial strain profiles for the two tests are depicted in Figure 2. The rupture temperature for HBR#2 falls within the alpha-beta transition temperature range. According to NUREG-0630, cladding strain typically decreases in the alpha-beta region following a balloon burst, before increasing again in the beta region. Thus, the strain results for HBR#2 align with the experimental data reported in NUREG-0630 [3]. Additionally, the rupture geometries for both tests are consistent. This observation aligns with data reported in Powers and Meyer [3], which indicates that smaller balloons generally lead to smaller rupture openings in both length and width.

Table 2. Summary of the HBR#2 Post LOCA test measurements in comparison to HBR#1

Parameter	**HBR#1**	**HBR#2**
Temperature at burst (°C)	770	850 - 870
Hold temperature (°C)	1,000	900
Burst shape	Oval	Oval
Burst length (mm)	7	8.4
Max. burst width (mm)	~2	1.5
Max strain $(\Delta C/Cm)_{max}$ (%)	25	20

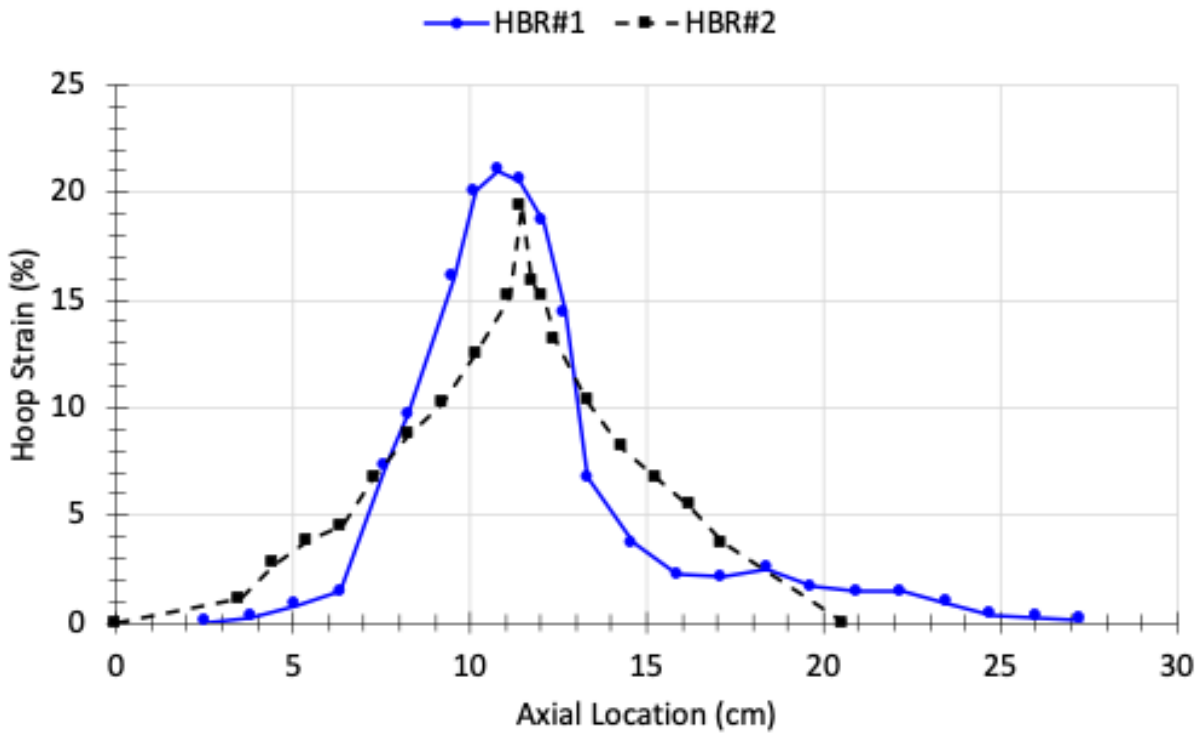

Figure 2. HBR#2 posttest hoop strain measurements as a function of axial location from the bottom of the rod.

After the test, dispersed fuel was collected from the LOCA test rig. It was observed that minimal material was gathered following the rupture event. The rodlet was then removed from the rig for visual inspection (see Figure 3) and to measure cladding strain as a function of axial location. After inspection and measurement, the sample was placed horizontally and rolled to evaluate the extent of material dispersion through the rupture. The dispersed material was collected and combined with the post-LOCA dispersed material. Next, the rodlet was sectioned at the mid-plane where the rupture occurred. Mobile fuel was extracted from both ends of the sample and set aside for sieving. Images of this process are shown in Figure 3b and 3c. The amount of fuel removed from the sample was assessed using the rod, and cladding strain thresholds were identified. Results indicated a possible cladding strain threshold of 8.16% for the top of the rod and 12.5% for the bottom, as shown in Figure 4. Finally, the fuel was sieved to determine the size of the fragments removed.

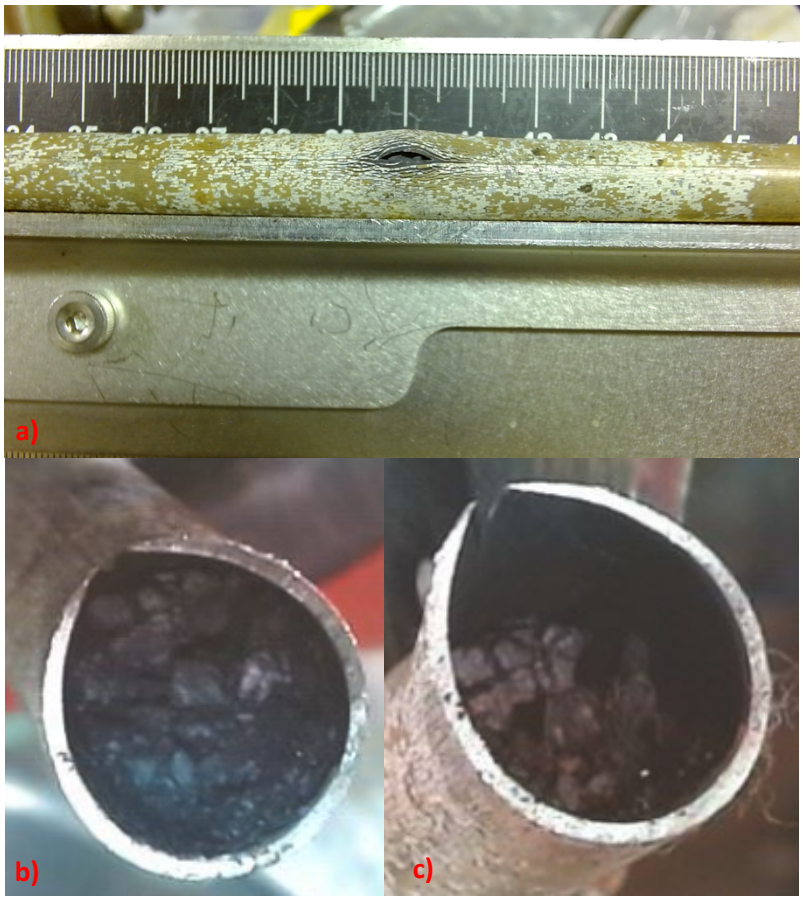

Figure 3. HBR#2 posttest images a) complete sample, b) bottom section post sectioning, and c) top section post sectioning.

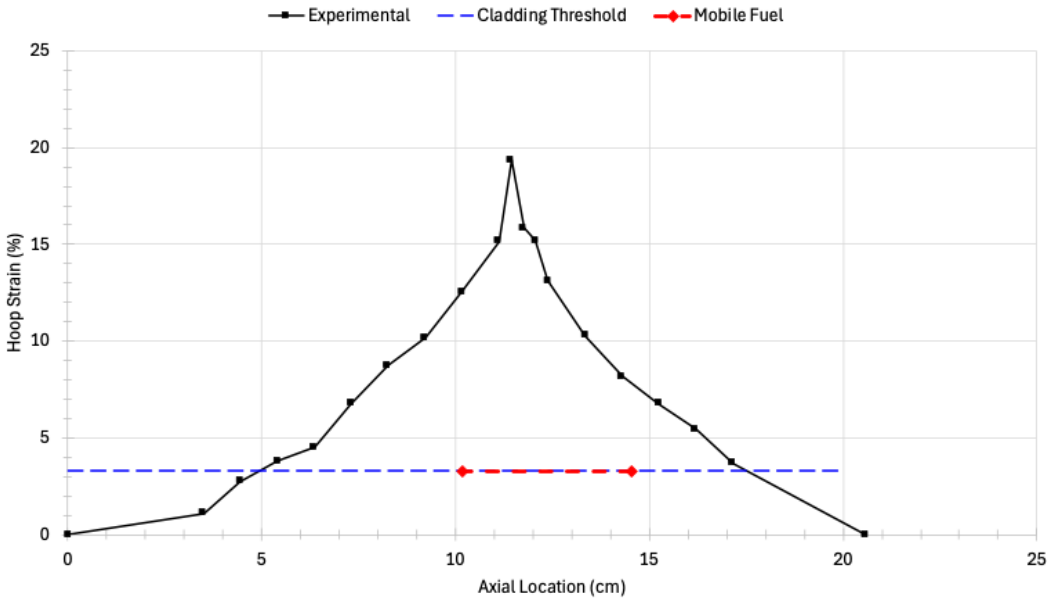

Figure 4. Mobile fuel removed from segment following sectioning and dumping of the fuel rod. Top strain = 8.16% and bottom strain = 12.5%.

The results from the sieving process are summarized in Table 3. Sieving was performed in two stages. In the first stage, material collected from both the LOCA test train and the rolling process was combined due to the limited quantity of dispersed material from the rodlet. This combined material is referred to as HBR#2 (Dispersed). In the second stage, the mass of material removed after sectioning the rodlet was sieved and weighed separately. The total mass removed from the rodlet, shown as HBR#2 (Total), was calculated by adding the masses from both stages. Comparatively, less fuel was removed from HBR#2 than from HBR#1. Specifically, HBR#2 contains approximately 33% less fuel than HBR#1. To facilitate a more accurate comparison, the total mass of fuel removed from the rodlet was normalized against the mass prior to the test. This normalization indicates that the percentage of fuel removed from HBR#2 is 20% lower than that of HBR#1. This difference could be attributed to the lower terminal temperature during the test. However, it is important to consider that the rupture temperatures and cladding strain profiles for HBR#2 and HBR#1 are significantly different, making it difficult to determine how these factors impact the amount of fragmented fuel removed. Figure 5 shows the normalized particle size distribution of the removed fuel. This analysis reveals that the fragments from the HBR#2 test are smaller than those from HBR#1. The reasons for this change in fragment distribution are not fully understood but may be related to differences in rupture temperature, cladding strain profile, or a combination of both factors.

Table 3. Summary of the HBR#2 fuel sieve data in comparison to HBR#1

Particle Size (mm)	Fuel Mass (g)		
	HBR#1	HBR#2 (Total)	HBR#2 (Dispersed)
>2	32.65	3.83	0
1	8.5	2.76	0.1
0.5	4.8	2.19	0.13
0.25	4	1.55	0.13
0.125	9.8	0.76	0.14

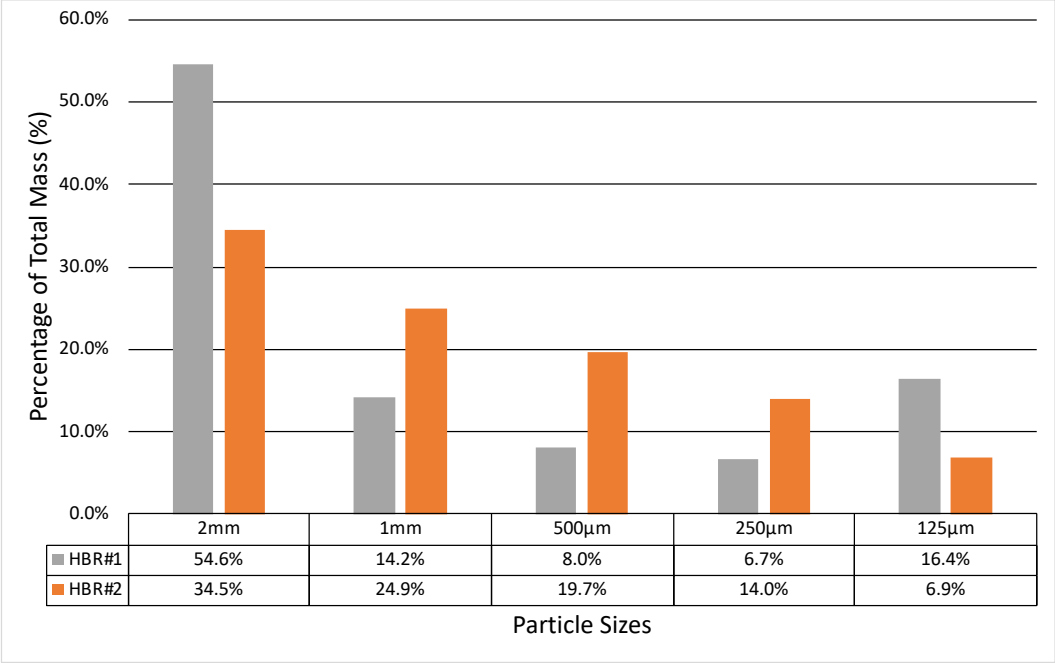

Figure 5. Particle size breakdown of removed fuel in % total mass.

2.2 RUPTURE TEMPERATURE BISON ANALYSIS

The BISON fuel performance code was employed to investigate the discrepancy in rupture temperatures between HBR#1 and HBR#2 and to understand the differing performance characteristics. This investigation involved two BISON LOCA simulations, differing only in their boundary conditions on the inner cladding surface. In the first simulation, the experimentally measured pressure from Figure 1 was applied. The second simulation used an 8.27 MPa pressure at 300°C and allowed BISON to adjust the pressure based on cladding deformation and gas temperature. The results are summarized in Table 4. Cladding rupture was assessed by comparing BISON's calculated hoop stress and temperature to the rupture criteria outlined in NUREG-0630. The simulation using experimental pressure predicts cladding rupture at 773°C, which matches the rupture condition for HBR#1. This result, based on the thin-walled tube approximation, aligns with expected rupture conditions. However, this prediction deviates by approximately 100°C from the experimentally measured rupture temperature for HBR#2.

One hypothesis is that this difference may be due to insufficient gas communication between the rodlet's internal gas and the external pressure lines. To test this theory, the second simulation assumed that the rodlet contained only the initial gas pressure provided at a specific temperature, and BISON was used to predict cladding failure and deformation based on this evolving system. This simulation predicts cladding failure around 878°C, which is only 8°C above the measured rupture temperature. A noted discrepancy is in the cladding strain, as shown in Figure 6. Both simulations predict similar cladding deformation, which is expected given that BISON's deformation model focuses on high-temperature creep without accounting for plastic instability. Consequently, BISON tends to underestimate balloon deformation, a limitation previously documented in related studies [4].

Table 4. BISON burst predictions using the experimentally measured pressure as a boundary condition versus an initial pressure with a small plenum

	Rupture Temperature (°C)	Peak Hoop Strain (%)
Experiment	850–870	20
BISON – Experimental Pressure Boundary Condition	773	6.7
BISON – Calculated Pressure Boundary Condition	878	4.8

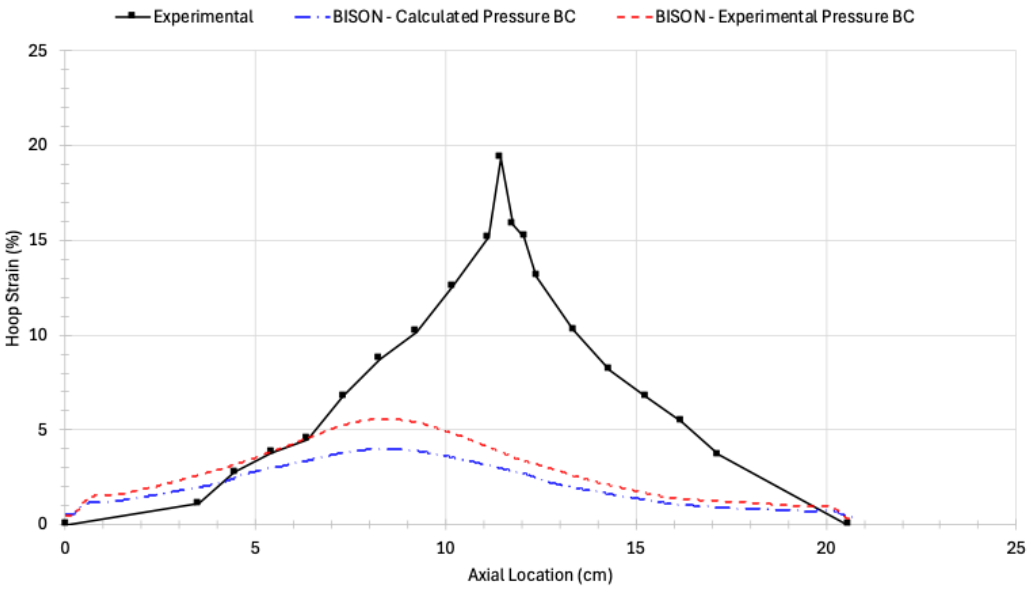

Figure 6. BISON-predicted hoop strain as a function of axial location.

3. IMPACT OF GRID SPACERS ON CLADDING AND HIGH BURNUP FFRD

3.1 OUT-OF-CELL CLADDING BALLOONING BEHAVIOR

Three out-of-cell LOCA tests were performed on 12 in. cladding segments to provide a baseline understanding of the impact of spacer grids during transient heating events. Two configurations were assessed, as shown in Figure 7. Configuration 1 was assessed to understand the impact of the rupture event, which typically occurs in the center of the cladding axial length. A 3×3 grid was sectioned from a spacer grid and positioned 1 in. above the cladding centerline. Thermocouples were placed 2 in. above and below the cladding centerline, and a third thermocouple was positioned in between the spacer grid and the cladding OD. Configuration 2 was proposed to force interaction between the cladding balloon event and the spacer grid segment through positioning of the spacer grid directly in the cladding centerline. Specimens for both Configurations 1 and 2 were internally pressurized to 8.3 MPa and subjected to LOCA-type conditions. The specimens were first heated to 300°C and held for 5 min to equilibrate the specimen temperature and simulate a prototypic operating temperature. Steam was injected into the system during this anneal step to flow around the exterior of the specimen. Next, specimens were exposed to a 5°C/s heating rate until cladding rupture, at which point the furnace power supply was shut off and specimens were cooled to room temperature.

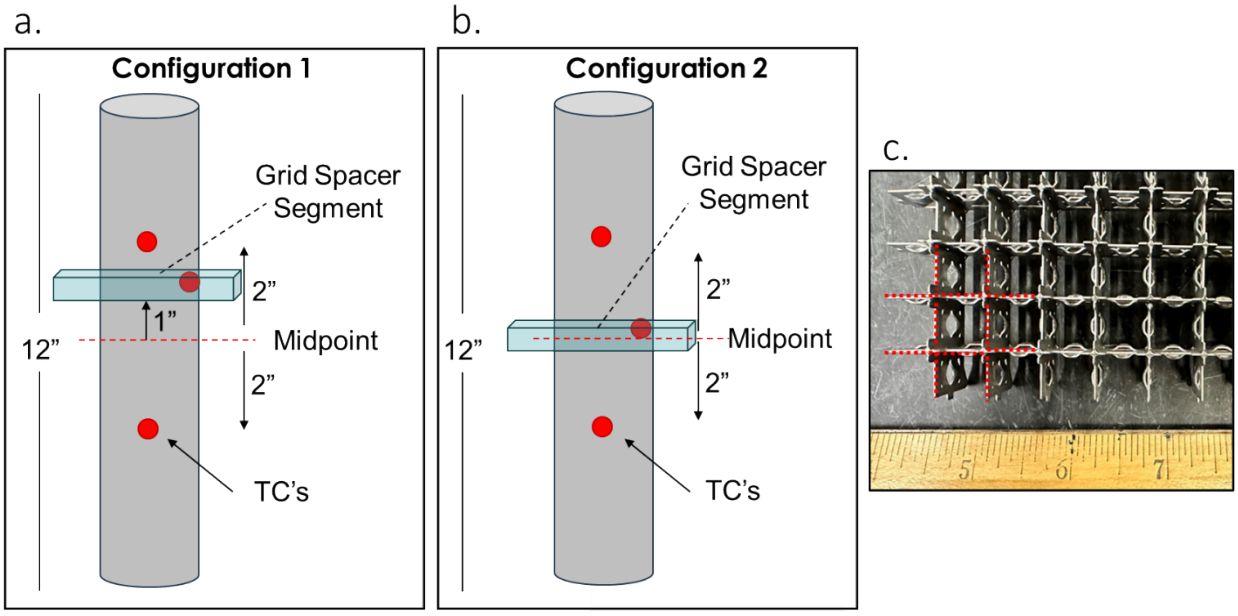

Figure 7. Out-of-cell grid spacer and thermocouple test configuration. a. configuration 1, b. configuration 2, and c. spacer grid, where the spacer segment used in testing was a 3×3 grid as shown by the red dashed lines.

Figure 8a shows the specimen from Configuration 1 after the LOCA rupture test. Rupture occurred in the center of the specimen closest to the lower thermocouple. The temperature distribution across the specimen during the test is shown in Figure 8. The thermocouple nearest rupture showed the highest temperature across the axial length of the cladding. The thermocouple 2 in. above the cladding centerline was dramatically cooler in temperature than the rupture area, likely due to a combination of IR shielding from the spacer grid and turbulent steam flow above the spacer grid location. Calipers were used to measure the maximum diameter change across the axial length of the cladding, shown in Figure 8c. The lower thermocouple shows clear constriction of deformation near the hot zone. Additionally, the spacer grid also limited strain to less than 1% in the hoop direction.

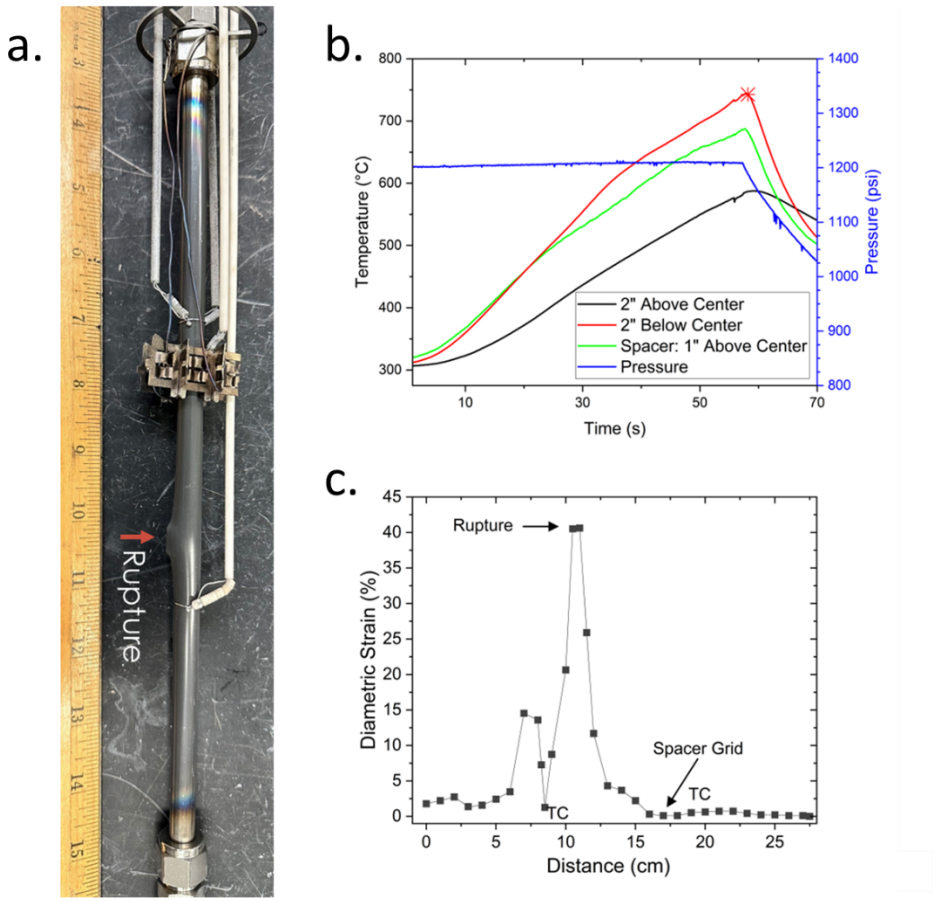

Figure 8. Configuration 1 out-of-cell test results. a. ruptured cladding, b. temperature and pressure profiles, and c. post-test diametric strain measurements from calipers. TC refers to wire-wrapped thermocouple positions.

Configuration 2 also showed rupture nearest to the thermocouple 2 in. below the cladding centerline, Figure 9a. Adjustment of the spacer grid to the centerline provided some forced interaction between the spacer and rupture site. With increased distance between the external thermocouples and the centerline spacer grid segment, the thermocouples 2 in. above and below the cladding centerline showed similar temperature profiles, as shown in Figure 9b. The centerline of the cladding underneath the spacer grid segment was again cooler than the rupture location. The depressed temperature, along with the constriction of the cladding from the spacer grid, resulted in minimal deformation under the spacer grid, shown in Figure 9c.

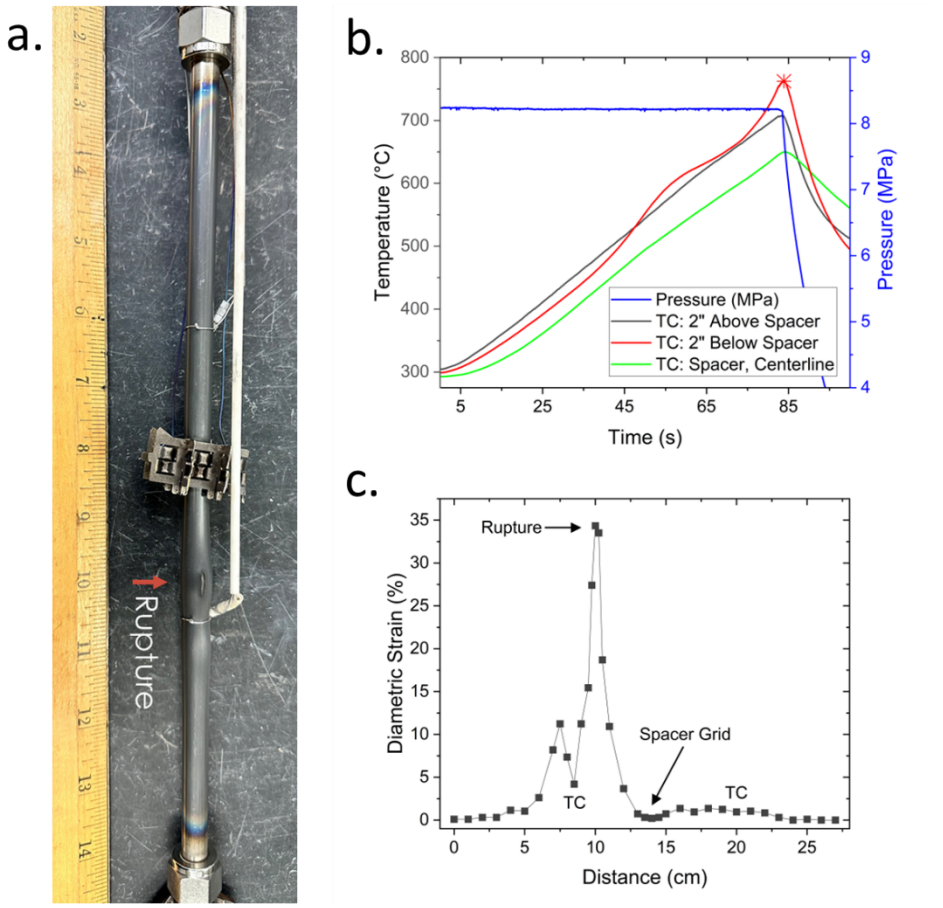

Figure 9. Configuration 2 out-of-cell test results. a. ruptured cladding, b. temperature and pressure profiles, and c. post-test diametric strain measurements from calipers. TC refers to wire-wrapped thermocouple positions.

A 3D laser scanner was developed for implementation into the hot cell for analysis of cladding deformation. Prior to hot cell implementation, the 3D laser scanner was compared against caliper measurements for both tests (Figure 10a and 10b). The laser scanner is shown in Figure 10c. The laser scanner collected data every 10° rotation around the tube for the entire axial length of the cladding. Due to this large rotational increment of 10°, high-strain regions of the tube, such as the rupture site, were not properly captured. Refinements can be made through use of smaller degree increments to capture both large- and small-magnitude deformation phenomena in the future. Yet, it is clear from both measurement devices that the spacer grid impacted local deformation of the cladding during the LOCA tests. The rupture width was decreased for Configuration 2, where the spacer grid was closer to the rupture site. Figure 11a and Figure 11b show a 3D light scanner reconstruction of half of the cladding surface and an optical image of the cladding under the spacer grid for Configuration 2 posttest. No evidence of deformation was visible, other than tube scratches from the spacer grid. Figure 11c provides profilometry across the axial length of the cladding visualized in Figure 11b, where clear constriction of the cladding is evident at the location of the spacer grid segment.

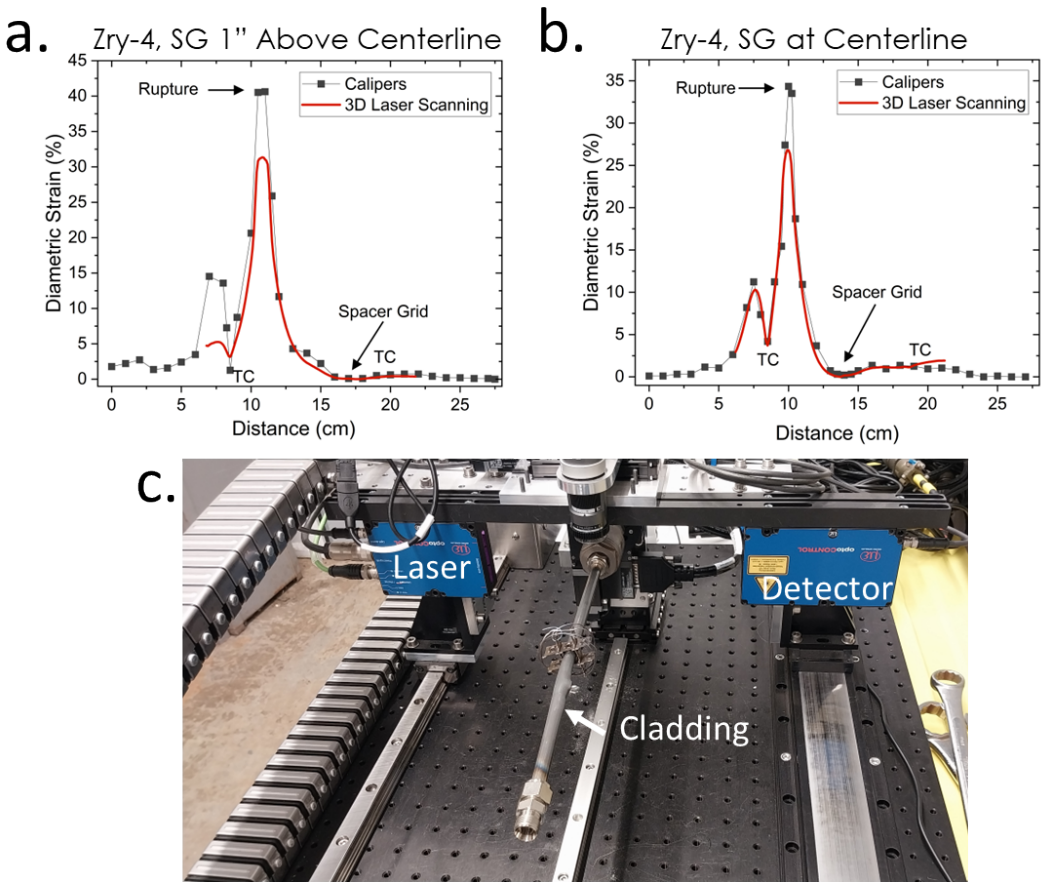

Figure 10. Posttest balloon deformation measurement comparison with calipers and 3D laser scanning. a. Configuration 1, b. Configuration 2, and c. hot-cell deployable laser scanner system.

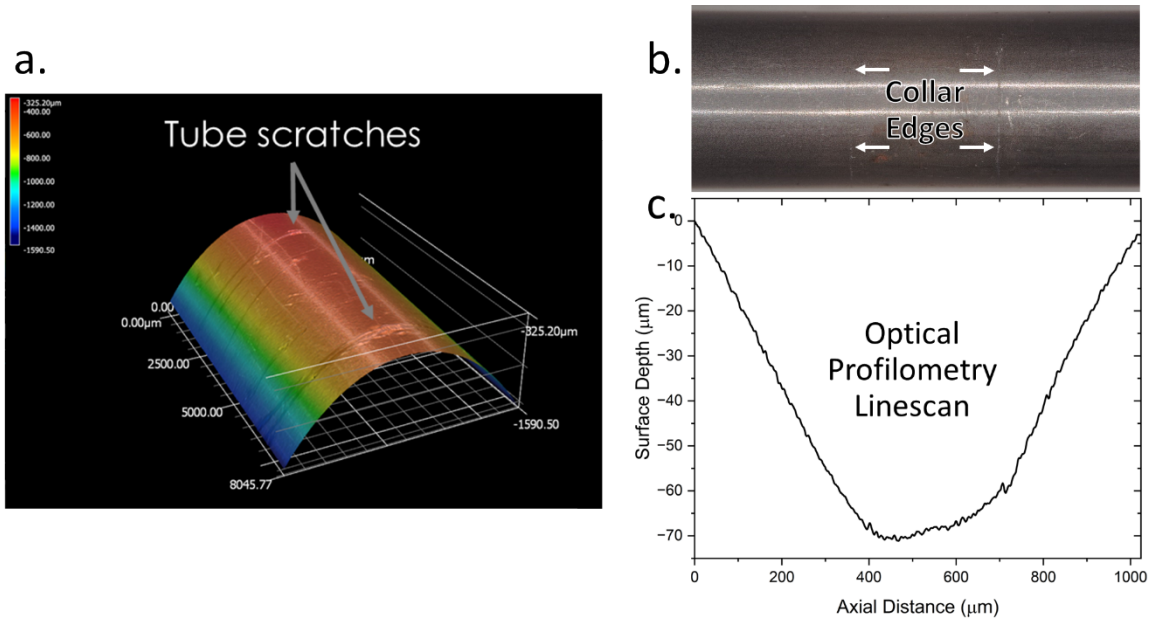

Figure 11. Configuration 2 optical analysis of the cladding region under the spacer grid. a. 3D surface reconstruction showing tube scratches, b. optical image of the collar scratches, and c. optical profilometry of the tube from (b).

The spacer grid segment utilized for initial demonstration testing provided context that the spacer grid would constrict ballooning during hot cell LOCA testing. To simplify the specimen build for hot cell operators, a stainless steel worm drive clamp was used as a surrogate for the spacer segment. This third validation test was performed to provide a test configuration (Figure 12a) and clamp type (Figure 12b) identical to those that would be utilized in the hot cell.

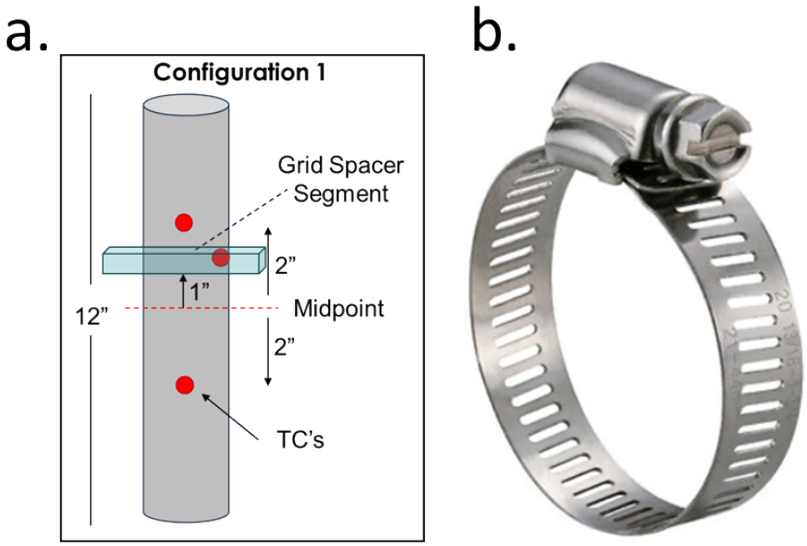

Figure 12. Out-of-cell benchmark for in-cell test a) test configuration and b) worm drive clamp representing a simulated grid spacer.

The test results for the out-of-cell benchmark test are shown in Figure 13. A similar temperature gradient was found 2 in. above and below the cladding centerline. An additional thermocouple was placed above the clamp so that the heat transport through the clamp could be analyzed. The clamp was found to absorb

more heat than what is transferred to the cladding surface under the clamp. The constriction from the clamp in addition to the lower temperature at the clamp region again resulted in negligible deformation in the hoop direction at the clamp location, shown in Figure 13b.

The cladding ruptured below the lowest thermocouple, and the balloon geometry was partially constrained by the thermocouple wire wrap 2 in. below the cladding centerline. Despite this wire wrap constriction, the rupture opening appeared symmetric in shape, inset within Figure 13b. This result implies that the rupture opening and the balloon geometry are not always directly correlated. Furthermore, rupture was found to occur at the hottest axial section of the cladding.

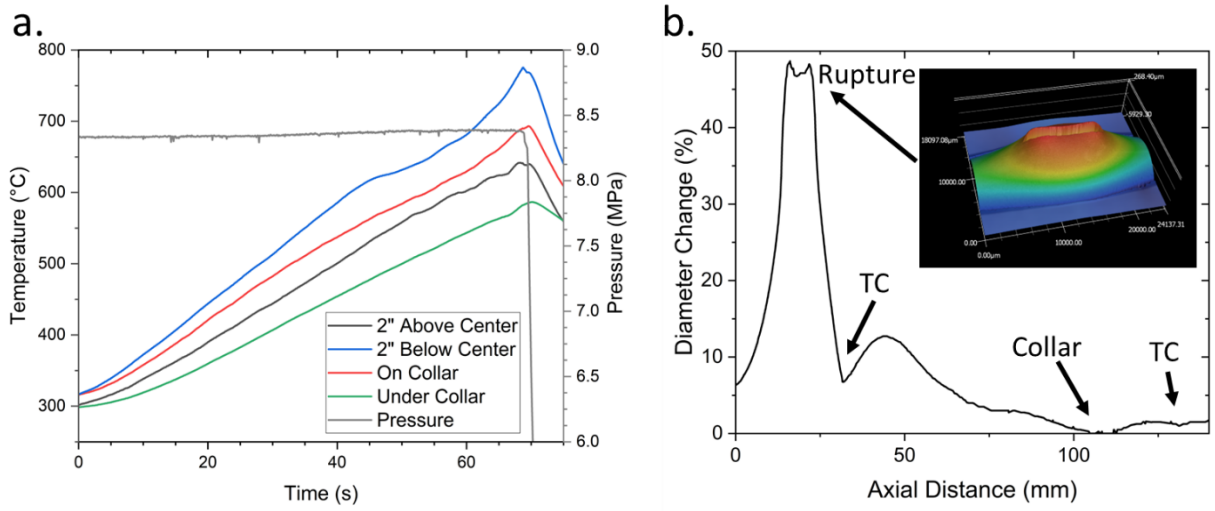

Figure 13. Test results for the out-of-cell benchmark for in-cell test. a) Pressure and thermocouple readings and b) cladding balloon deformation.

3.1.1 SATS Experimental Temperatures Compared to Thermal Hydraulic Experimental and Analytical Results

One concern with the SATS experiments is its comparison to prototypic LOCAs. A significant difference between SATS and a real LOCA is that SATS externally heats the cladding, whereas in a prototypical LOCA, the cladding experiences both internal and external heating resulting from decay heat. Additionally, the structural features of the assembly, such as grid spacers and mixing veins, locally suppress the power and burnup, and grid spacers and mixing veins are designed to enhance local heat transfer properties. Therefore, when evaluating the impact of assembly structural features on cladding performance and FFRD in-cell, it is crucial to ensure that the axial and local temperature conditions are consistent with expected real-world scenarios.

This behavior has been historically evaluated, and the best example of this evaluation is reported in NUREG/CR-4166. These tests involved a 3.9 m, 5×5, 25-rod bundle with solid heater elements inside the tubes. The heaters were designed to produce a flat chopped cosine power distribution along the full length of the bundle. Multiple tests were conducted to measure cladding temperature, both with and without grid spacers, at the same locations. The results, presented in Figure 3-3 of the NUREG report, indicate that tests with grid spacers resulted in cladding temperatures approximately 75°C cooler than those without grid spacers. A key conclusion from the experiment was that the fragmentation of larger water droplets enhanced cooling near the grid spacers. Although these rod designs are from an older generation, the results provide useful insights into expected local temperature conditions.

The experimental test was confined to a 5×5, 25-rod bundle, which, though significant, does not fully represent the complexities of a complete-core LOCA scenario. To address this, CTF was employed to evaluate the temperature evolution of fuel rod cladding during a full-core LOCA event. The CTF results

were derived from a VERA simulation of a high-burnup core undergoing a LOCA transient, enabling a comparison with experimental data and an assessment of how spacer grids affect cladding temperature behavior. A VERA model was developed for a four-loop pressurized water reactor (PWR) that was depleted to the end of its cycle using 24-month cycles [5,6]. Figure 14 illustrates the VERA power profile at the time of the LOCA, which was used by CTF to predict cladding temperature changes for the rod in question. The reflood phase of a large-break LOCA transient was simulated using this model in CTF, incorporating the VERA-predicted power distribution [7]. For this study, the CTF model was enhanced by increasing the axial nodalization from 24 to 49 levels, which improves the resolution of spacer grid heat transfer effects. The CTF model incorporates several specific models to capture thermal-hydraulic phenomena effectively, which are listed below.

- Droplet behavior
    - Entrainment and de-entrainment at the quench front and liquid film
    - Turbulent enhancement of heat transfer
    - Impingement heat transfer (droplets impacting the rod surface)
    - Interfacial heat transfer to superheated vapor
- Spacer grid effects
    - Convective heat transfer enhancement due to turbulent enhancement
- Heat transfer effects
    - Radiative heat transfer between rod and droplets/vapor
    - Convective and boiling heat transfer to liquid and vapor in dispersed flow film boiling and transition boiling heat transfer regimes

Some notable models that were not activated in this study are anticipated to cause additional impact on clad temperature behavior. The models, however, were not ready for assessment at the time of this study. These additional models are as follows.

- Spacer grid quenching (tracking of spacer grid film, droplet entrainment and de-entrainment)
- Radiative heat transfer between spacer grid and pins
- Spacer grid induced droplet breakup

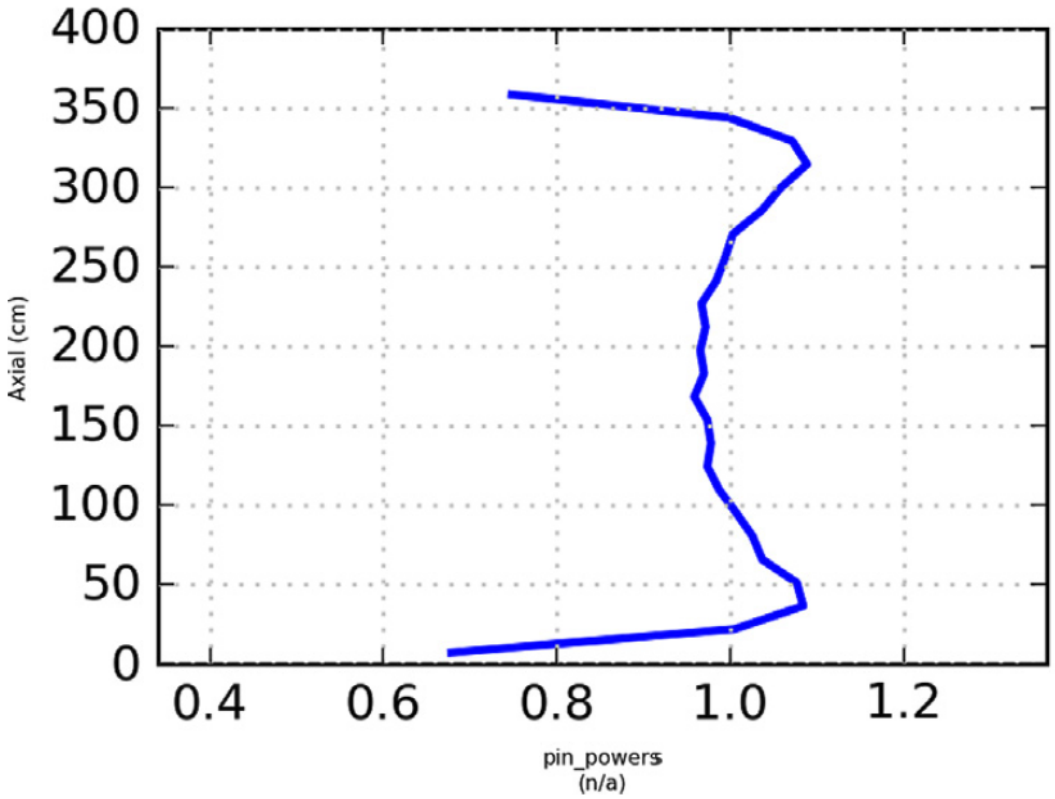

Figure 14. VERA-predicted power profile at the last hot full power condition [5-7].

Figure 15 presents the results of the CTF analysis for the time during a LOCA when the peak cladding temperature (PCT) was reached. This particular time was selected to highlight various phenomena observed during a LOCA and to illustrate the temperature differences along the rod's axial length. The initial observation is that the bottom of the rod has already been quenched, with the lower 1.5 m of the rod showing complete quenching. In contrast, the fuel rod above 1.5 m remains at high temperatures. The cladding temperature generally increases linearly until it reaches the top portion of the rod, where the decay heat is sufficiently low to decrease the temperature. An interesting stair-step pattern can be seen approximately every 20–30 cm, which corresponds to the spacing between grid spacers or mixing veins. These grid spacers or mixing veins locally reduce the cladding temperature due to decreased decay heat—see Figure 14—and enhanced heat transfer. Moving axially upward within a grid span, the temperature increases until about three-quarters of the way up the span, where it then starts to decrease. This pattern clearly illustrates the effect of grid spacers or mixing veins on local cladding temperatures. Fuel performance analyses indicate that this local temperature suppression is effective in preventing cladding ballooning [9]. The most uniform axial temperature distribution occurs near the PCT, with a temperature difference of approximately 10°C between the PCT and the temperature at the grid spacer/mixing vein locations. If the non-activated models were made active, this temperature difference might be even greater. Based on experimental and analytical analyses, the cladding–grid spacer temperature difference is expected to be in the 10–75°C range. The combined results from these two analyses, along with the final out-of-cell SATS benchmark results, provide strong confidence to proceed with in-cell testing on commercially irradiated material.

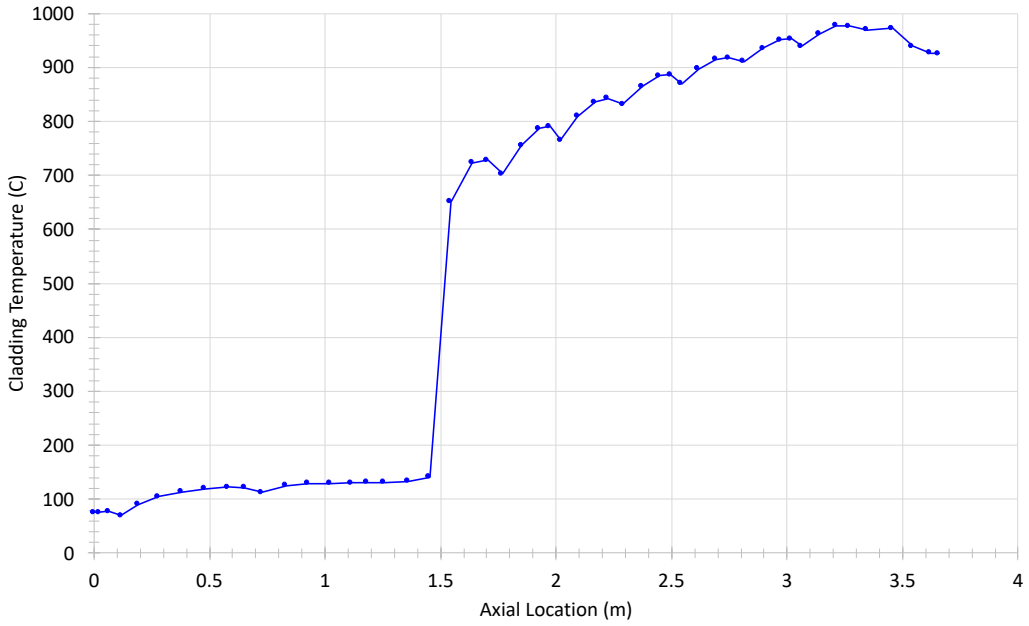

Figure 15. CTF axial temperature profile when the peak cladding temperature is reached.

3.2 IN-CELL HIGH BURNUP FFRD

3.2.1 North Anna Fuel Operating Conditions

The rods are identified hereinafter by the reactor in which they were operated; see Table 5. Table 5 provides a detailed summary of the fuel operating conditions and initial postirradiation examination results. The detailed operating conditions were provided by the utilities and vendors for use in the BISON fuel performance code. The North Anna (NA) fuel rod is one of three sibling rods being used in a high-burnup lead test rod program [8]. The rod operated in the central regions of the core for two cycles before being moved to the core periphery. The rod and its siblings were then removed from the original assembly and re-inserted into a new assembly. The new assembly was then inserted into the center of the core for a fourth cycle. A time-dependent average linear heat rate (ALHR) and local LHR at the axial location of interest can be found in Figure 16.

Table 5. Description of the North Anna fuel rod and operating conditions [8]

	Value	**Units**
Reactor Type	PWR	—
Number of Cycles	4	—
Cladding Type	M5	—
Initial Enrichment	4.2	%
Rod Average Burnup	63	MWd/tU
Sample Average Burnup (MWd/tU)	68	MWd/tU
Last Cycle LHR at the Axial Location of Interest	~15	kW/m
Nominal Outer Diameter	9.5	mm
Initial Wall Thickness	0.57	mm
Hydrogen Concentration	<120	Wt ppm
Measured FGR	9.8	%

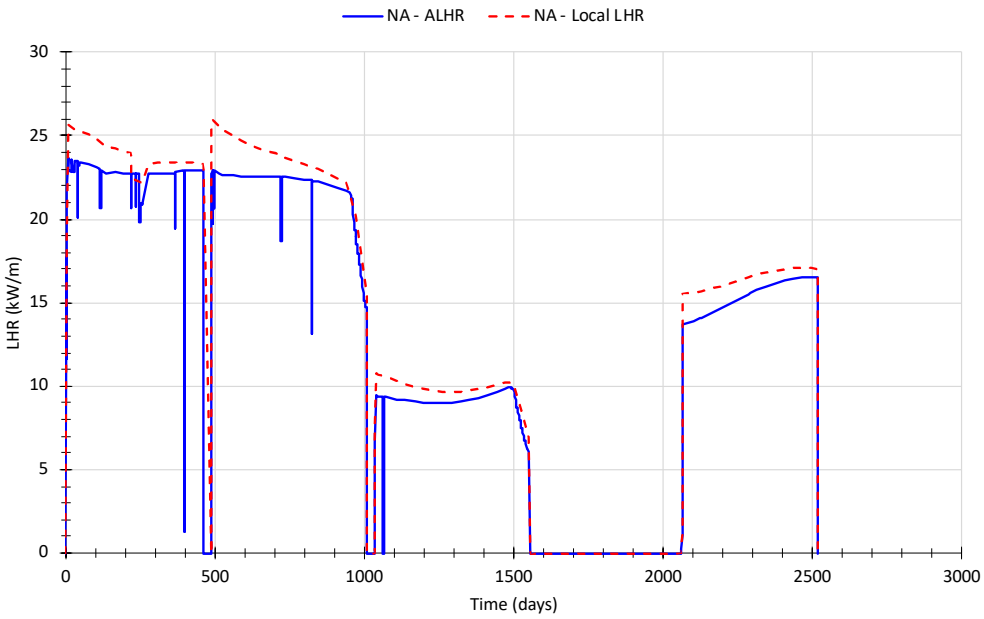

Figure 16. Rod average linear heat rate and local linear heat rate for the LOCA tested sample.

3.2.2 LOCA Test Conditions for In-Cell Test

The out-of-cell tests conducted on standard Zircaloy-4 alloys provided valuable insights into expected cladding temperature conditions and facilitated an informed design for the in-cell experiments. For these in-cell tests, we utilized the same experimental setup as shown in Figure 12, with a ring clamp representing the grid space. The ring clamp was selected for two key reasons: it replicates the temperature conditions reported by thermohydraulic experiments and analyses, and it is compatible with the hot cell's design, making it easier to apply to the rodlet.

Table 6 and Figure 17 summarize the test conditions and rupture temperature for the NA grid spacer LOCA test, and Figure 17 presents the online temperature and pressure readings during the in-cell LOCA test. These test conditions align with those of previous high-burnup LOCA tests. The rodlet, measuring 30 cm in length, was pressurized to 8.27 MPa at 300°C and heated at a rate of 5°C/s. The heating continued until the sample reached a terminal temperature of 1000°C, at which point the furnace was turned off, concluding the experiment. The online measurements, as depicted in Figure 17, confirm these conditions. Upon reaching 300°C, the sample was pressurized and held for 10 min to ensure stability. To maintain a constant gas pressure, a valve linking the rodlet system to a larger gas reservoir remained open throughout the test. This approach was chosen to reduce uncertainties in the test results. During the hold period, the pressure remained stable, as shown in Figure 17. At approximately 750 s, heating resumed in accordance with the specified conditions until the sample reached 1000°C, as indicated by the thermocouple readings. The pressure remained constant until the terminal temperature was achieved, after which a gradual pressure decrease was noted before the pressure valve was opened at around 900 s to depressurize the system. Cladding rupture was identified by analyzing the thermocouple data and detecting the characteristic discontinuity associated with rupture, which occurred at a reported temperature of 861°C.

Table 6. Summary of the NA grid spacer LOCA test conditions

Parameter	Value	Units
Rodlet Length	~30	cm
Environment	He	—
Internal pressure at 300°C	8.27	MPa
Temperature ramp from 300°C	5	°C/s
Terminal temperature	1,000	°C
Hold time	0	s
Rupture Temperature	861	°C
Rupture Width	0.64 / 0.64	mm
Rupture Length	4.7 / 5.6	mm

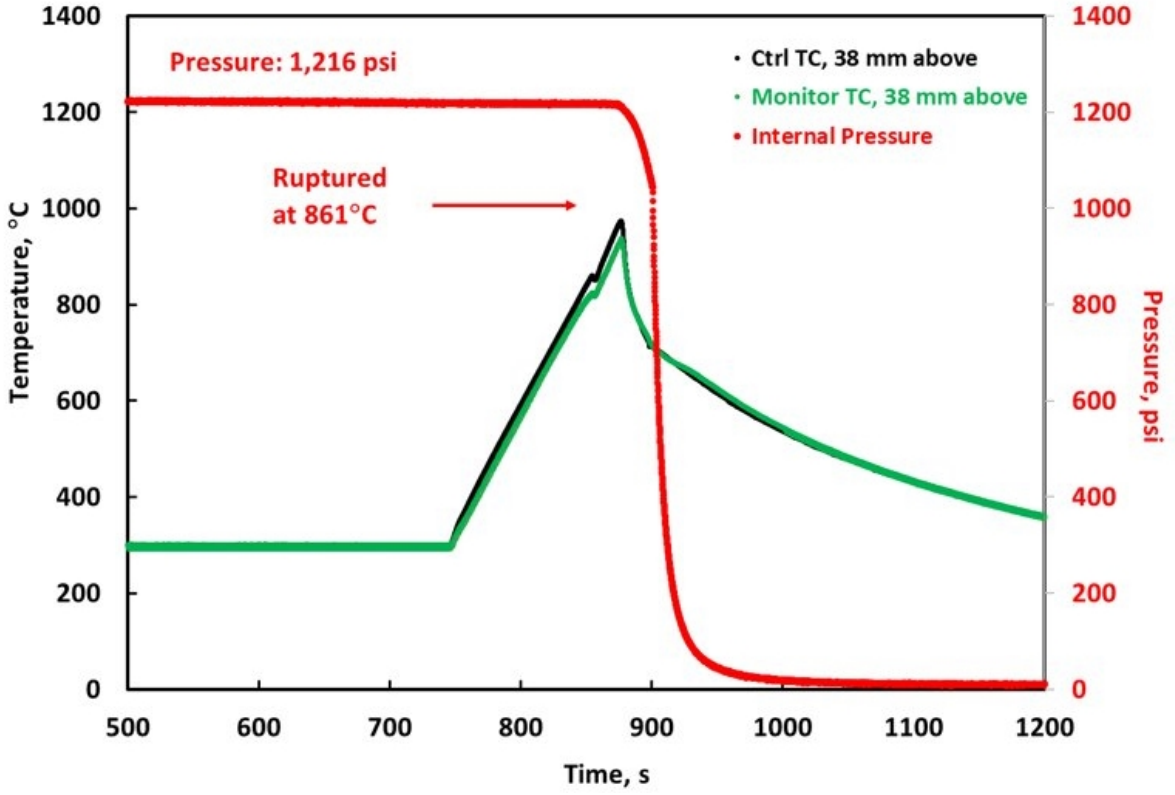

Figure 17. Time-dependent temperature and pressure measurements during North Anna grid spacer in-cell test.

3.2.3 Transient Fission Gas Release Data Collected During In-Cell Test

During the test, the transient fission gas release (tFGR) from the sample was evaluated. This was done by utilizing a system developed and tested previously; details about this system can be found in two reports by Yan et al. [11,12]. In this configuration, the quartz tube that surrounds the sample is continuously swept with helium. The helium travels in-cell, through the quartz tube, back out-of-cell, and then passes into the tFGR table, which includes a water trap followed by a cold trap, where ^{85}Kr and other fission gasses are absorbed on activated charcoal that is kept at liquid nitrogen temperatures. Helium then exits the table and is returned to the hot cell. The cold trap was continuously monitored by a sodium iodide (NaI(Tl)) detector. The NaI detector monitored the count rate in the trap and the quantitative ^{85}Kr activity in the cold trap in 5 min intervals. After burst occurs in the sample, fission gas is transported out of the quartz tube and through the tFGR table. This evaluates the integral tFGR for the entire transient. The transient is faster than the response time of the tFGR table. Any tFGR that occurs post burst is also

captured by the table. An alternative test configuration would be required to capture temperature-dependent tFGR.

The response of the tFGR system to this test is plotted in Figure 18. In this test, gas from the burst filled the entire system temporarily before it could transport through the tFGR table. This delayed collection of the ^{85}Kr at the trap. Gas release from the burst began to arrive at the trap approximately 15 seconds after the burst and can be seen as rate meter counts rising approximately 1800 s after the start of the test. The rate meter rise from ~1000s to 1800s was due to ^{137}Cs contamination. The ^{85}Kr activity continued to rise over the next 20 min until it reached a steady activity of 23.36 µCi. Based on the best available data, the fuel segment that was tested contained 0.52 Ci of ^{85}Kr at the time of the test. The fractional tFGR for this test is then 5.1%. This fractional release is consistent with other measurements of tFGR [10,14-16] and lower than that of other tests performed previously with this system that were not under pressure, which further matches expectation for literature [17].

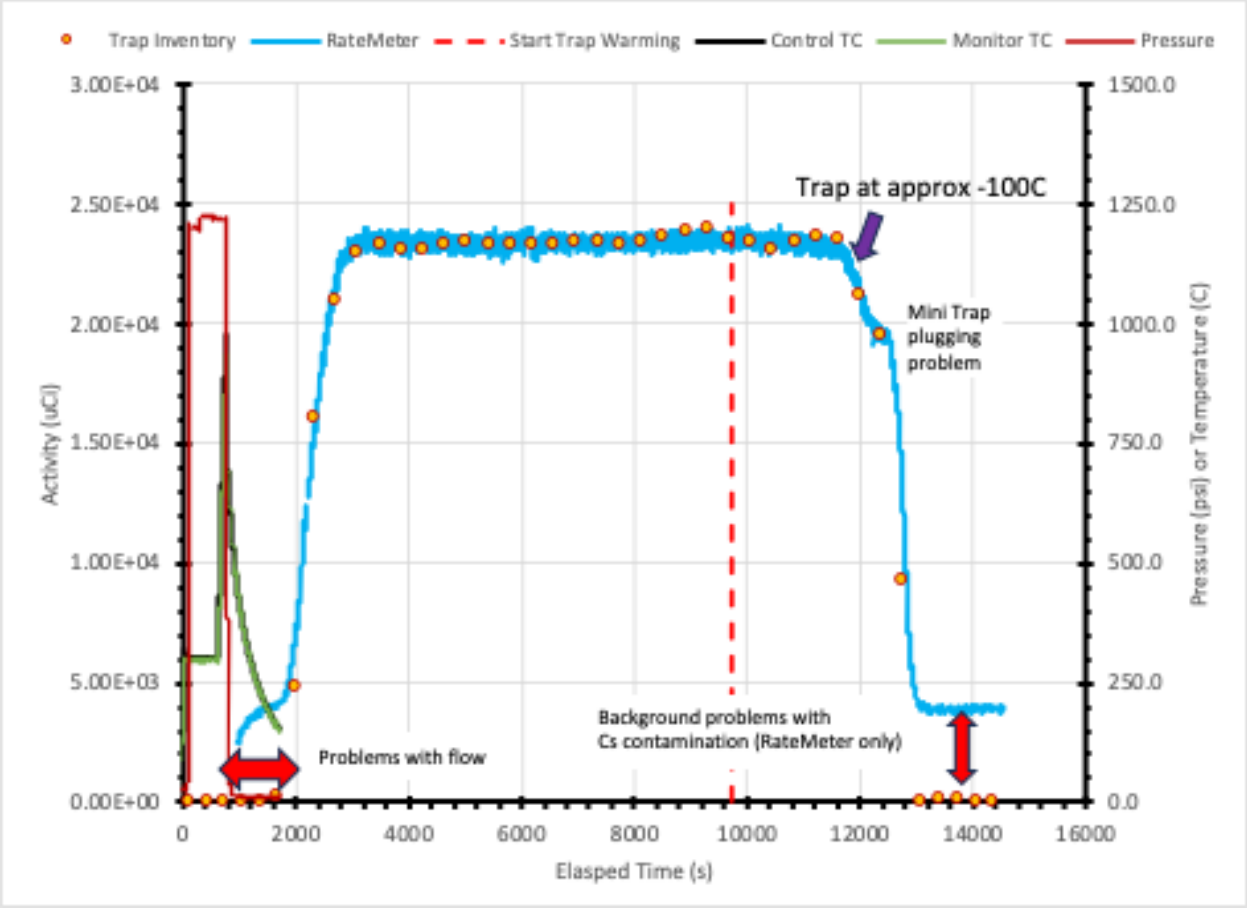

Figure 18. Online activity measurement from the in-cell North Anna grid spacer tests.

3.2.4 Post-Test Characterization

Post-LOCA images of the rodlet and the dispersed material during the simulated LOCA are shown in Figure 19 and Figure 20. Figure 19 presents three images detailing the rod's condition, highlighting the formation of two distinct balloons. The first balloon, positioned to the left of the clamp, is located near the top of the sample, approximately 1.4 cm from the clamp. The second balloon, situated to the right of the clamp, is closer to the bottom of the sample, around 2.54 cm from the clamp, and nearer to the center of the furnace heating zone. Ruptures were observed at both balloon locations, with close-up images of each rupture shown in Figure 19b and c. The rupture openings are relatively small: the rupture above the clamp

measures 4.7 mm in length and 0.64 mm in width, whereas the rupture below the clamp measures 5.6 mm in length and 0.64 mm in width. These measurements are also detailed in Table 6.

It is important to note that the double rupture observed in this test is unusual compared to other in-cell tests. There are several theories regarding the formation of these balloons. One theory suggests that the first rupture occurred below the clamp in the center of the furnace, the hottest region. The clamp may have obstructed or at least restricted gas flow between the upper and lower regions of the rodlet. As a result, gas from the upper region, combined with the large system volume, could not depressurize effectively. This led to ballooning and eventual rupture in the upper region due to the sustained pressure. This scenario contrasts with a full-length fuel rod, where the gas volume is orders of magnitude smaller, and the large gas reservoir is typically situated half a meter to a meter away from the anticipated rupture location.

Figure 20 shows the fuel dispersed during the LOCA test, which was then collected for weighing and sieving. This dispersed fuel, mainly comprising fine fragments, represents only a small fraction of the total mass in the rodlet. Additionally, the mobile fuel from both the upper and lower regions of the rodlet were removed, weighed, and sieved. A measuring utensil was also used to assess the cladding strain threshold. These three data sets are presented later in this report.

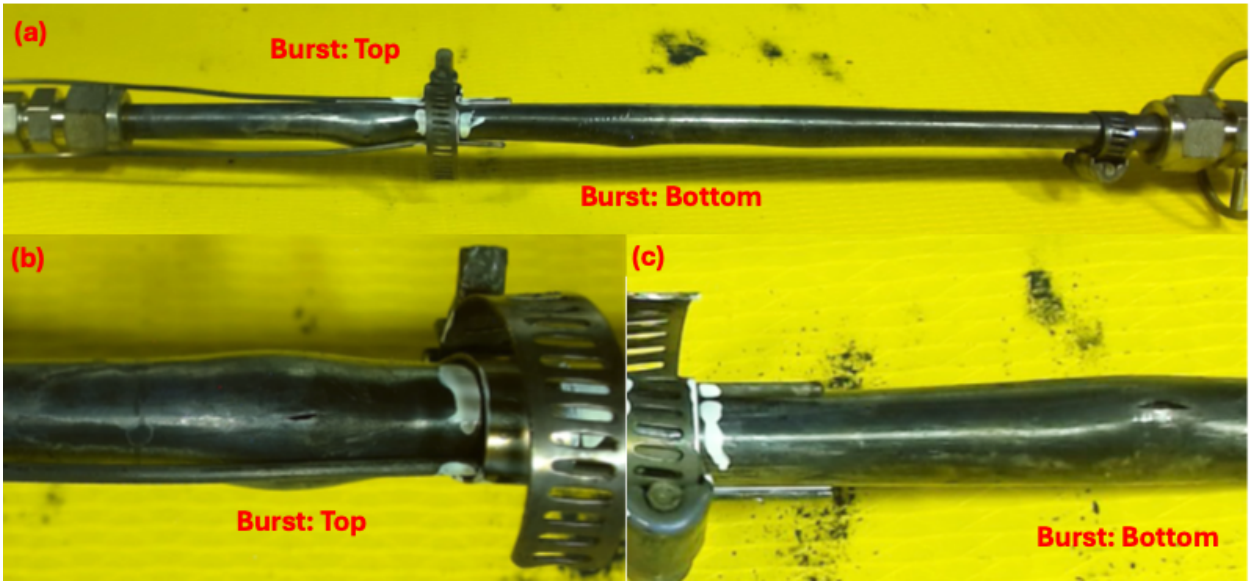

Figure 19. Post LOCA images of the NA grid spacer. a) The whole rod indicating a balloon and rupture on each side of the clamp, b) close up image of the top rupture, and c) close up image of the bottom rupture.

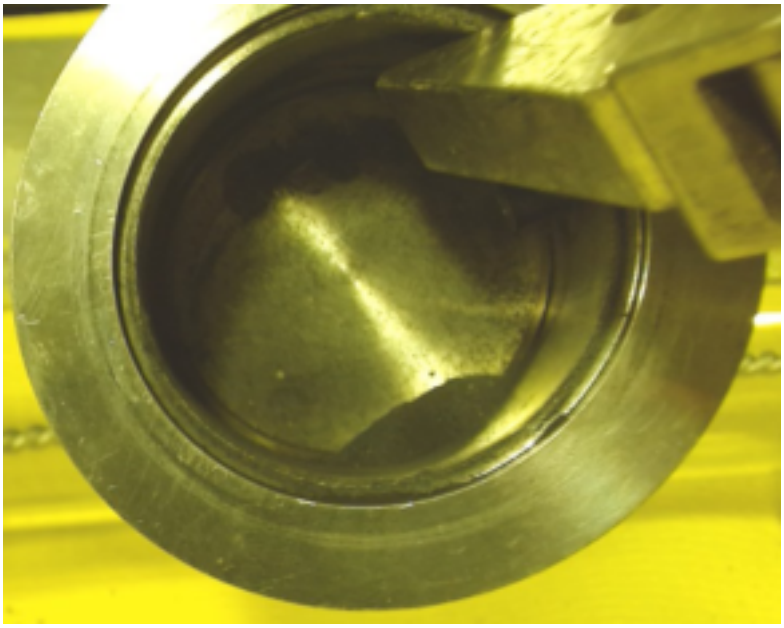

Figure 20. Image showing the fuel dispersed during the simulated LOCA transient, primarily consisting of fine fragments.

Before sectioning, measurements of cladding profilometry and rupture openings were recorded and are presented in Figure 21 and Table 6. Figure 21 provides a detailed view of these measurements. Figure 21a offers an overview of the sample, marking the balloon or high strain regions and spacer grid locations with solid lines for reference in the profilometry data. Figure 21b summarizes the measurements taken at both the 0° and 90° positions relative to the identified ruptures, whereas Figure 21c shows the average of these two data sets. The data reveal three distinct balloon regions identified by peak strain values. Although the two balloons shown in Figure 19 were readily visible, the third balloon was only detected through strain measurements. Notably, the third balloon appears more uniform around the tube compared to the other two, which exhibited some asymmetry. This uniformity suggests that the third balloon did not develop a rupture, indicating that the local material did not reach a point of plastic instability. Additionally, the two balloons with rupture locations are larger than the third balloon, suggesting that they experienced higher stresses or temperatures.

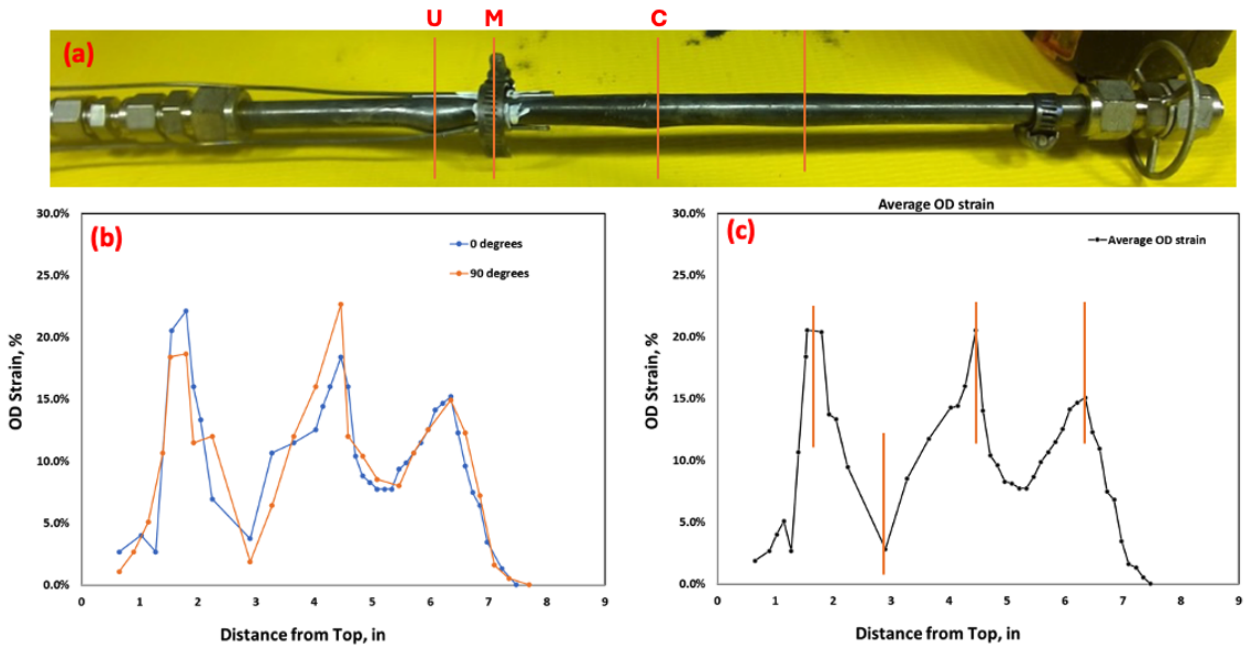

Figure 21. Description of the a) cladding segment with notable features, b) measurements taken at 0° and 90°, and c) average cladding strain.

Following diametral strain measurements, the sample was cut into three pieces to retrieve the remaining mobile fuel for fragmentation analysis. The rodlet was sectioned at two specific locations, as outlined in the cutting diagram shown in Figure 21a. The first cut, referred to as "1st cut" in Figure 22, was made at the lower burst region (labeled C in Figure 21a). The second cut, termed "2nd cut" in Figure 22, was at the upper burst region above the clamp (labeled U in Figure 21a). Images of each cut section were taken immediately after sectioning, as shown in Figure 22. The images reveal that the fuel was fractured into a large fragment; some portions were pulverized but were still retained in their original location. However, the fuel was loose at both ends and easily removed when the segmented samples were dumped. The fragmented fuel was collected in three stages: first, from the dispersal during the LOCA event; second, from the fuel that fell out of both ends of the segments. Notably, material collected from the upper and lower segments was kept separate. After initial collection, the segments were stored together. Over time, additional fuel loosened during transport and was collected. As the segments were stored together, it was not possible to determine the source of the additional dislodged material. Future postirradiation examinations will involve cutting a specimen at the clamp location (labeled M in Figure 21) for optical microscopy to determine whether the fuel remained confined by the clamp.

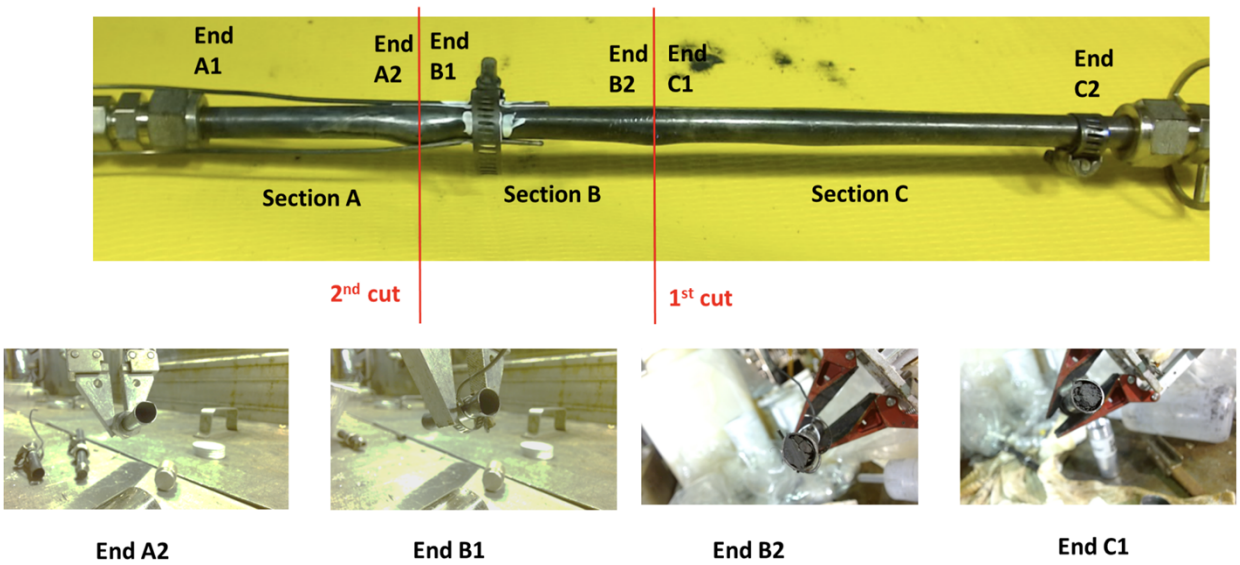

Figure 22. Images depicting the sample cutting diagram and the cross sections of all cuts performed on the sample.

After sufficiently removing the mobile fuel from the rodlet, a measuring tool was used to assess the distance to the remaining fuel within the rod. This measurement, plotted alongside the cladding profilometry data, helps determine the cladding threshold that prevents the fuel from becoming mobile after a LOCA event. The results of this analysis are shown in Figure 23, with measurements indicated by red dots connected by a red dashed line. Note that there are two sets of measurements: one for the top segment and one for the bottom segment. Importantly, the two sets do not connect, suggesting that fuel remains at the clamp location and indicating that the clamp may locally prevent FFRD. Optical micrographs of the clamped region will provide further insight into fuel behavior and assess whether the clamp effectively mitigates FFRD. In the upper region, two distinct cladding strain thresholds appear to be present: at approximately 5.1% above the rupture and around 9.5% below it. Conversely, in the lower region, the cladding strain threshold above the rupture is about 8.5%, whereas below the rupture the fuel is removed almost down to the Swagelok, with a cladding strain threshold close to 0%. This variation in behavior is likely due to the formation of a third balloon between 5 and 7 in. from the top of the rodlet, which would have provided additional space for fuel relocation within the rodlet. Conversely, the presence of the third balloon may have made it more difficult for fuel below the rupture to disperse, as the fuel would tend to fall rather than rise. However, it is impossible to assess this probability because it was not possible to perform gamma scanning on the sample. Future work should consider performing gamma scanning if multiple balloons are observed.

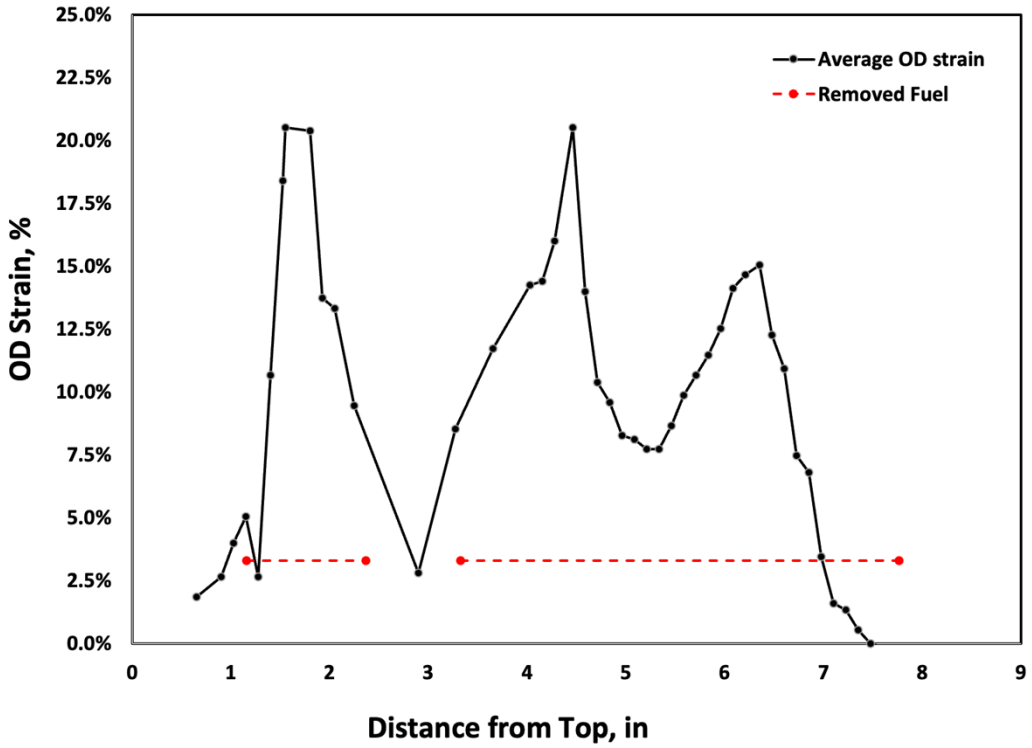

Figure 23. Mobile fuel removed from segment following sectioning and dumping of the fuel rod. Upper segment: top strain = 5.1% and bottom strain = 9.5%. Bottom segment: top strain = 8.5% and bottom strain = ~0%.

The collected material was weighed and sieved, and the results are detailed in Table 7. During the LOCA event, 0.8 g of fuel was dispersed, which represented approximately 0.47% of the total rodlet mass. After sectioning, 11 g of fuel was extracted from the section "above the clamp," and 18 g from the section "below the clamp," corresponding to roughly 6.6% and 10.8% of the rodlet's total fuel mass, respectively. An additional 22.17 g of material was obtained from the entire fuel segment after it was stored and handled within the hot cell. The specific source (upper or lower) of this additional material remains unknown. In total, 67.5 g of fuel was removed from the rodlet, representing about 40.6% of its total mass. It is important to note that although this total reflects the mass of material removed, only 0.8 g was ejected during the LOCA burst event. These results are illustrated in Figure 23, with the particle size distribution categorized to match historically reported values. The key observation is that the majority of the material removed (58.1 g) was retained above 2 mm and was extracted only after sectioning. Conversely, most of the material dispersed during the LOCA event was smaller than 0.125 mm.

Table 7. Summary of the North Anna grid spacer fuel sieve data

Particle Size (mm)	Fuel Mass (g)				
	Dispersed at Burst	Above the Clamp	Below the Clamp	Removed during Transport	Total Removed
>4.75	0	7.8	7.8	9.8	25.4
3.35-4.75	0	7.6	1.5	14.9	24
2.0-3.35	0	1.1	0.9	6.7	8.7
1.0-2.0	0	0.5	0.4	2	2.9
0.425-1.0	0.1	0.5	0.3	1.8	2.7
0.25-0.425	0	0.2	0	0.9	1..1
0.106-0.25	0.1	0.2	0	1	1.3
0.53-0.106	0.3	0.1	0.1	0.4	0.9
<0.053	0.3	0	0	0.2	0.5
Total Mass	**0.8**	**11**	**18**	**37.7**	**67.5**
Mass Removed / Initial Fuel Mass (%)	**0.47**	**6.6**	**10.8**	**22.17**	**40.6**

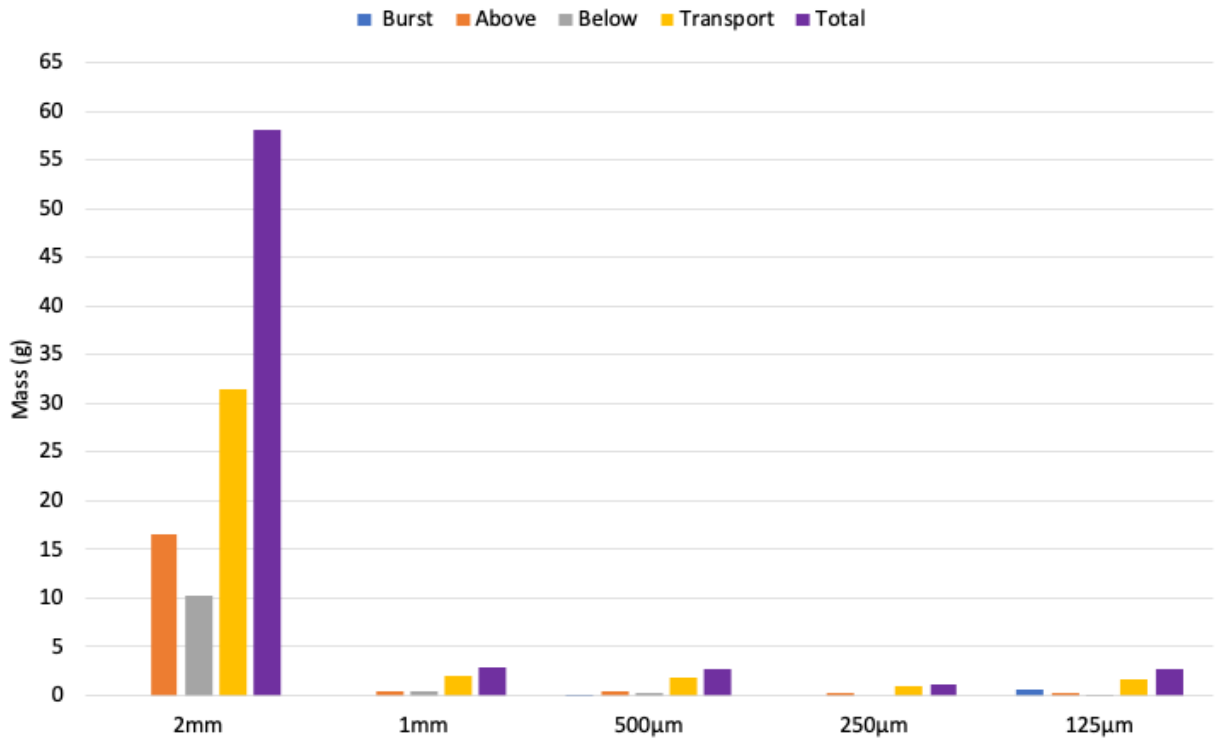

Figure 24. Breakdown of the removed particle size as a function of mass and method of removal.

4. LOCA TESTS ON BYRON SAMPLE 6XV-5E

4.1.1 Byron 6XV Fuel Operating Conditions

Table 8 provides a detailed summary of the fuel operating conditions and initial postirradiation examination results. The detailed operating conditions were provided by the utilities and vendors for use in the BISON fuel performance code. The Byron 6XV fuel rod is one of seven sibling rods being used in a high-burnup and accident-tolerant fuel lead test rod program [18]. The rod operated in the central regions of the core for two cycles before being re-inserted into a new assembly and placed back into the center of the core. A time-dependent ALHR and local LHR at the axial location of interest can be found in Figure 25.

Table 8. Description of the North Anna fuel rod and operating conditions [8]

	Value	Units
Reactor Type	PWR	
Number of Cycles	3	
Cladding Type	Adv. Zry Alloy [18]	
Rod Average Burnup	73.7	MWd/tU
Last Cycle LHR at the Axial Location of Interest	~15	kW/m
Nominal Outer Diameter	9.144	mm
Initial Wall Thickness	0.575	mm
Measured FGR	13.3	%

Figure 25. 6XV rod average linear heat rate as a function of time.

4.1.2 LOCA Test Summary

Unlike the previous two LOCA tests, this test aimed to evaluate the effects of pre-heating the sample before conducting the LOCA test. Previous tFGR tests involved heating secured samples to assess tFGR, followed by introducing an axial slit into the cladding. Observations indicated that fragmentation during subsequent heating was significantly lower compared to that of samples that were only heated once and had an axial slit. However, these tests were conducted on single or double pellets and might not fully represent a LOCA scenario. Thus, this test was designed to replicate those conditions more

comprehensively. A ~21.6 cm rodlet from Byron 6XV was used to construct a LOCA test train. The rodlet was heated in a steam environment to 1000°C, after which the furnace was turned off and the sample was allowed to cool. Discussions have raised concerns about tFGR's potential to cause ballooning and premature cladding rupture. According to NUREG-0630, even minimal pressure can lead to cladding ballooning and rupture at 1000°C. Therefore, any significant tFGR could result in cladding deformation, and possibly ballooning and rupture.

To evaluate this effect, the sample was not initially pressurized to determine whether tFGR alone could cause cladding deformation. Post-heating measurements showed no change in the cladding's outer diameter. The sample was then reinserted, pressurized to 11 MPa, and subjected to a prototypic LOCA experiment. The LOCA test was concluded when cladding rupture occurred. Detailed summaries of the heating and LOCA tests are provided in Table 9, and Figure 26 displays the thermocouple and pressure measurements recorded during the heating test (Figure 26a) and the LOCA test (Figure 26b). Images of the sample were taken following the LOCA test; see Figure 27. The first observation is that the rod is severely bent, with the rupture occurring on the concave side of the rodlet. This suggests that the rupture was caused by a force sufficient to bend the rod. Whether this is a typical occurrence remains to be seen, as reactor rods, which are 3.6 m (12 ft) long, are designed with grid spacers and mixing veins every 20–60 cm (8–24 in.) to prevent bending. Postirradiation examination is currently underway and is expected to be completed in the coming months. This analysis will include cladding profilometry, examination of rupture geometry, weighing and sieving of dispersed and mobile fuel, and optical microscopy of various regions of the rodlet.

Table 9. Summary of the NA grid spacer LOCA test conditions

Parameter	Value	Units
Rodlet Length	~21.6	cm
Environment	Steam	—
Unpressurized Temperature Transient		
Internal pressure at 300°C	Atm	atm
Temperature ramp from 300°C	5	°C/s
Terminal temperature	1,000	°C
Hold time	0	s
Pressurized LOCA Transient		
Internal pressure at 300°C	11.0	MPa
Temperature ramp from 300°C	5	°C/s
Terminal temperature	782	°C
Hold time	0	s
Rupture Temperature	782	°C

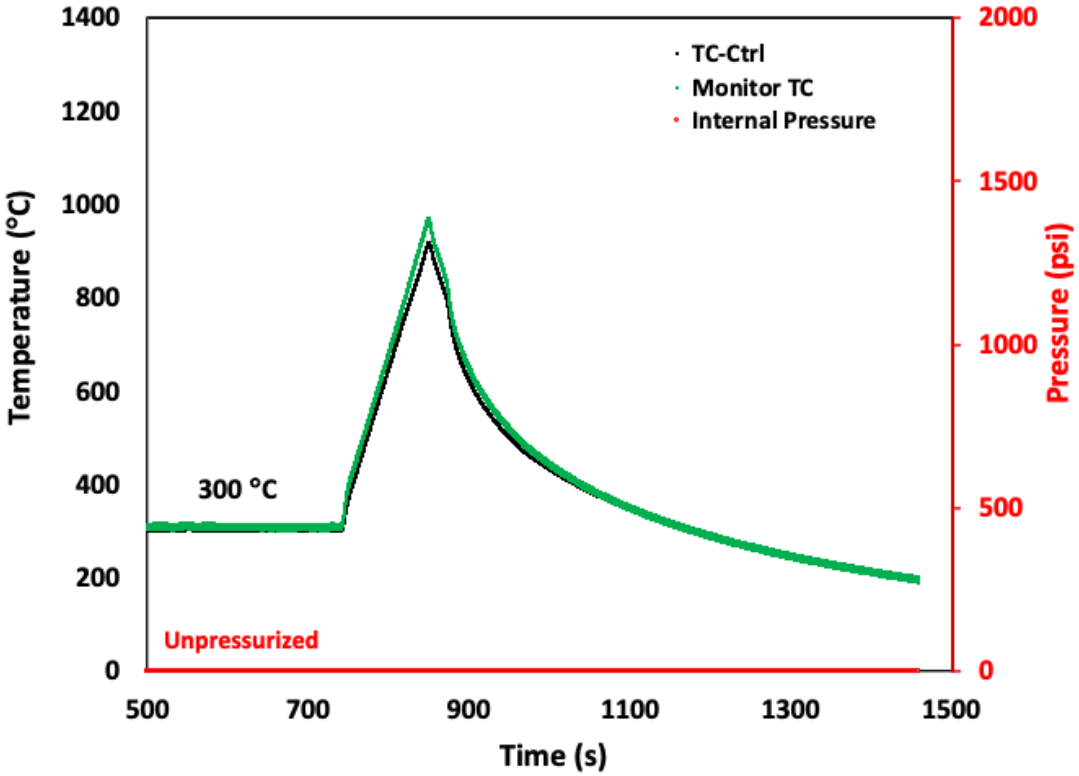

a)

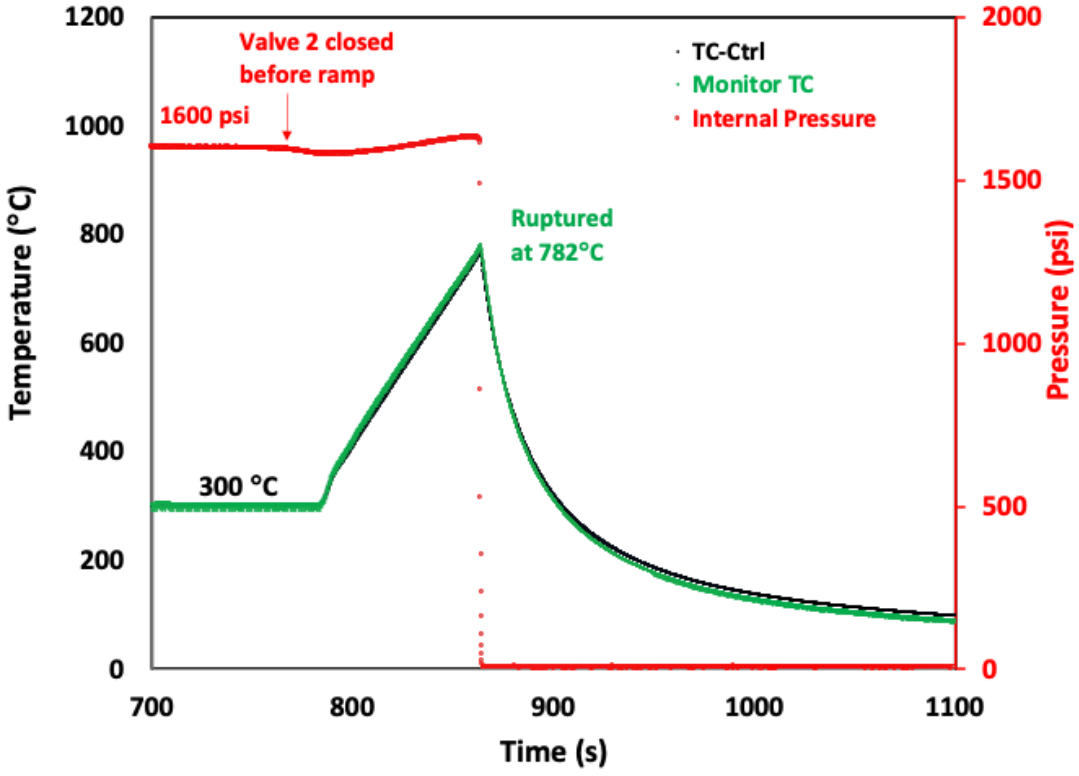

b)

Figure 26. a) Time-dependent temperature during the unpressurized heating stage and b) time-dependent temperature and pressure measurements during the Byron 6XV-5E LOCA test.

Figure 27. Image of sample 6XV-5E following LOCA testing.

5. CONCLUSIONS

Three LOCA tests were conducted at the ORNL SATS facility to address data gaps and key questions concerning the industry's high-burnup safety case. The first test aimed to evaluate the impact of terminal temperature on FFRD. For this test, material from the same rods was used, the only variation being the length of the rodlets: one was 30 cm long, and the other was approximately 20.5 cm. In the tests, HBR#1 was heated to a terminal temperature of 1000°C, whereas HBR#2 was heated to 900°C. HBR#2 exhibited significantly less FFRD compared to HBR#1, despite the shorter rodlet length. However, HBR#2 also had a rupture temperature of approximately 100°C higher than that of HBR#1. BISON simulations were employed to investigate the differences in cladding performance between the two samples. It was found that HBR#2 experienced gas communication issues between the rodlet and the gas in the lines where the pressure transducer was placed. This issue led to a reduced gas volume during the LOCA test and ultimately resulted in an increased cladding rupture temperature for HBR#2. Consequently, it remains uncertain whether the observed differences in FFRD behavior were due to the terminal temperature or the increased rupture temperature.

The second test was one of the most complex LOCA tests conducted to date. Its purpose was to evaluate how assembly structural features influence FFRD behavior. These structural features are designed to provide mechanical stability and enhance heat transfer. To ensure that the test is representative, out-of-cell experiments were conducted to evaluate various methods for simulating a grid spacer and to confirm that cladding conditions at and around the grid spacer matched expectations. The results from these out-of-cell tests were compared with experimental data and CTF simulations, and the measured cladding temperatures fell within the ranges reported by both the thermal hydraulic experiments and CTF simulations. Consequently, a ring clamp was selected for the in-cell test. The in-cell test, which included the complex LOCA test train with the ring clamp, also recorded time-dependent tFGR at the moment of burst. These data are intended to help the industry assess how tFGR might impact cladding burst.

The in-cell test was successfully conducted under conditions similar to those reported previously [2]. As before, the NA grid spacer ruptured at a higher-than-expected temperature. Two rupture openings were observed, and three balloons were ultimately measured. tFGR measurements were successfully obtained and appeared to be lower than those reported in the NRC FFRD Research Information letter [10] under similar burnup conditions. Fuel sieving was performed in multiple stages to evaluate dispersal at the time of rupture, and fuel was removed from both the upper and lower segments of the rodlet to assess the impact of the double rupture. PIE will continue with the objective of studying fuel behavior in the vicinity, which will involve optical microscopy. A section diagram has been developed to guide the completion of PIE on this rodlet.

The final test evaluated the effects of pre-heating on FFRD. The sample, obtained from the 6XV Byron reactor that had been previously irradiated, was heated to 1000°C without internal rod pressure to investigate whether tFGR would lead to cladding deformation, ballooning, or rupture. No such deformation was observed, and the cladding's outer diameter remained consistent with measurements taken before heating. Following this, the sample was pressurized to 11 MPa and heated until rupture occurred. The rupture event caused significant bending of the sample, likely due to the high pressure. Due to time constraints, not all post-test data could be collected, but further data collection is anticipated and will be detailed in a future peer-reviewed publication.

6. REFERENCES

1. C. McKinney, R. Seibert, J. Werden, C. Parish, T. Gerczak, J. Harp, N. Capps, Characterization of the radial microstructural evolution in LWR UO2 using electron backscatter diffraction, Journal of Nuclear Materials, Volume 585, 2023, 154605, ISSN 0022-3115, https://doi.org/10.1016/j.jnucmat.2023.154605
2. N. Capps, Y. Yan, A. Raftery, Z. Burns, T. Smith, K. Terrani, K. Yueh, M. Bales, K. Linton, Integral LOCA fragmentation test on high-burnup fuel, Nuclear Engineering and Design, Volume 367, 2020, 110811, ISSN 0029-5493, https://doi.org/10.1016/j.nucengdes.2020.110811
3. Powers, D.A. and R.O. Meyer, Cladding swelling and rupture models for LOCA analysis, in NUREG-0630, 1980, U.S. NRC.
4. N. Capps, M. Ridley, Y. Yan, S. Bell, K. Kane, BISON validation to in situ cladding burst test and high-burnup LOCA experiments, Annals of Nuclear Energy, Volume 191, 2023, 109905, ISSN 0306-4549, https://doi.org/10.1016/j.anucene.2023.109905
5. I. Greenquist, A. Wysocki, J. Hirschhorn, N. Capps, Multiphysics analysis of fuel fragmentation, relocation, and dispersal susceptibility–Part 1: Overview and code coupling strategies, Annals of Nuclear Energy, Volume 191, 2023, 109913, ISSN 0306-4549, https://doi.org/10.1016/j.anucene.2023.109913
6. J. Hirschhorn, I. Greenquist, A. Wysocki, N. Capps, Multiphysics analysis of fuel Fragmentation, Relocation, and dispersal Susceptibility–Part 2: High-Burnup Steady-State operating and fuel performance conditions, Annals of Nuclear Energy, Volume 192, 2023, 109952, ISSN 0306-4549, https://doi.org/10.1016/j.anucene.2023.109952
7. R. Salko, A.Wysocki, B. Hizoum, N. Capps, A study on the impact of using a subchannel resolution for modeling of large break loss of coolant accidents, Annals of Nuclear Energy, Volume 207, 2024, 110716, ISSN 0306-4549, https://doi.org/10.1016/j.anucene.2024.110716
8. D. Jadernas, K. Yueg, M. Bales, D. Wachs, K. Terrani, K. Linton, N. Meacham, Sample selection report for the irradiation and post irradiation examination of ultra-high burnup fuel, INL/EXT-17-44054, January 2018
9. D. Schappel, N. Capps, Impact of LWR assembly structural features on cladding burst behavior under LOCA conditions, Nuclear Engineering and Design, Volume 418, 2024, 112887, ISSN 0029-5493, https://doi.org/10.1016/j.nucengdes.2023.112887
10. RIL 2021-13, "Interpretation of Research on Fuel Fragmentation, Relocation, and Dispersal at High Burnup," December 2021
11. Y. Yan, J.M. Harp, C. Baldwin, R.N. Morris, N.A. Capps, SATS Transient Fission Gas Release Test with Irradiated Fuel under Loss of Coolant Accident Conditions, Oak Ridge Natl. Lab. Rep. (2023) ORNL/SPR-2023/3154. https://doi.org/10.2172/2203029
12. Y. Yan, C. Baldwin, J.M. Harp, A. J. James, K. D. Linton, and N.A. Capps, SATS Transient Fission Gas Release Capability and Design, Oak Ridge Natl. Lab. Rep. (2022) ORNL/SPR 2022/2653
13. Y. Pontillon et al. "Experimental and Theoretical Investigation of Fission Gas Release from UO_2 up to 70 GWd/tU under Simulated LOCA Type Conditions." *Proc 2004 Int. Meeting on LWER Fuel Performance*, paper 1025, Orlando, Florida, September 19–22 (2004).
14. M. Marcet et al., Contribution of high burnup structure to fission gas release under transient conditions, paper 2005, Proc. Top Fuel, Paris, France, 6–10 September (2009).
15. M. Marcet, Etude de la fracturation mecanique de la structure a haut de combustion des combustible irradies (RIM) en traitement thermique, Universite d'Aix-Marseille December 2010, https://www.theses.fr/2010AIX22124/document
16. INTERNATIONAL ATOMIC ENERGY AGENCY, Advanced Fuel Pellet Materials and Designs for Water Cooled Reactors, IAEA-TECDOC-1416, IAEA, Vienna (2004)

17. J.A. Turnbull, S.K. Yagnik, M. Hirai, D.M. Staicu, C.T. Walker, An Assessment of the Fuel Pulverization Threshold During LOCA-Type Temperature Transients, Nucl. Sci. Eng. 179 (2015) 477–485. https://doi.org/10.13182/NSE14-20
18. Olson, L., Pitruzzella, E., Walters, J., Roberts, E., Mitchell, D., Mueller, A., Hallman, L., Pan, G., Metzger, K., Maier, B., Lyons, J., Jaworski, A., Lahoda, E., Kobelak, J., Shockling, M., Capps, N., Harp, J., (2022). Accident Tolerant and High Burnup Hotcell PIE at ORNL. 156-160. 10.13182/TopFuel22-38919.